American Mineralogist, Volume 74, pages 58–76, 1989

Redox equilibria, structure, and properties of Fe-bearing aluminosilicate melts: Relationships among temperature, composition, and oxygen fugacity in the system Na_2O-Al_2O_3-SiO_2-Fe-O

BJORN O. MYSEN, DAVID VIRGO
Geophysical Laboratory, 2801 Upton St., N.W., Washington, D.C. 20008, U.S.A.

ABSTRACT

Redox ratios of Fe and structural positions of Fe^{3+} and Fe^{2+} in melts in the system Na_2O-Al_2O_3-SiO_2-Fe-O have been determined with Mössbauer spectroscopy. The value of $\log(Fe^{2+}/Fe^{3+})$ generally is linearly correlated with $\log f_{O_2}$ and $1/T$ (T in kelvins). The Fe^{2+}/Fe^{3+} ratio decreases linearly with increasing Al/(Al + Si) and, for NBO/T > 0.4, the Fe^{2+}/Fe^{3+} ratio decreases with increasing NBO/T of the melt (NBO/T = nonbridging oxygens per tetrahedrally coordinated cation). The inverse correlation of Fe^{2+}/Fe^{3+} with Al/(Al + Si) is more pronounced at higher temperatures and with f_{O_2} reduced below that of air. The free energy of reduction of Fe^{3+} to Fe^{2+} increases (becomes less negative) with decreasing Al/(Al + Si) and NBO/T. With $Fe^{3+}/\Sigma Fe > 0.6$, Fe^{3+} is tetrahedrally coordinated ($^{[4]}Fe^{3+}$), whereas for $Fe^{3+}/\Sigma Fe < 0.3$, Fe^{3+} occurs in octahedral coordination ($^{[6]}Fe^{3+}$). In the $Fe^{3+}/\Sigma Fe = 0.6$–0.3 range, tetrahedral and octahedral Fe^{3+} coexist. Fe^{2+} generally is a network modifier.

The degree of polymerization of silicate liquids depends, therefore, on $Fe^{3+}/\Sigma Fe$. The NBO/T generally will increase with increasing temperature, decreasing f_{O_2}, and decreasing Al/(Al + Si). For properties that depend on degree of melt polymerization, these properties will also be functions of $Fe^{3+}/\Sigma Fe$. An example of such a property is melt viscosity where the activation energy of viscous flow decreases with increasing NBO/T. For melts in the system Na_2O-Al_2O_3-SiO_2-Fe-O with 5 wt% iron oxide added as Fe_2O_3, the viscosity decreases by more than 40% in the $Fe^{3+}/\Sigma Fe$ range between 1.0 and 0.0. The temperature dependence of the viscosity is more pronounced than in Fe-free melts with the same Al/(Al + Si), in which NBO/T does not depend on temperature.

The results are combined with published experimental data from simple synthetic and complex natural liquids to show that in natural magmatic liquids the proportion of $^{[4]}Fe^{3+}$ increases systematically as the liquids become more felsic. For example, Fe^{3+} in anhydrous rhyolite melts is predominantly in tetrahedral coordination, whereas Fe^{3+} in basaltic and picritic melts principally exists in octahedral coordination. Thus, during fractional crystallization of basaltic liquids toward felsic melt compositions, the $^{[4]}Fe^{3+}/^{[6]}Fe^{3+}$ ratio will increase.

INTRODUCTION

Natural magmatic liquids commonly have appreciable concentrations of iron oxide (Fe_2O_3 and FeO). The Fe^{3+} in such melts may be both a network former and a network modifier (Mysen, 1987). Because Fe^{2+} generally occurs in octahedral coordination (e.g., Mao et al., 1973; Nolet et al., 1979), reduction of network-forming Fe^{3+} to Fe^{2+} results in changes in degree of polymerization of silicate melts. For example, with tetrahedrally coordinated Fe^{3+}, reduction to octahedrally coordinated Fe^{2+} results in an increase in NBO/T (i.e., melt depolymerization), whereas reduction of octahedrally coordinated Fe^{3+} to octahedrally coordinated Fe^{2+} is associated with a decrease in NBO/T. Melt properties that are related to melt polymerization—such as viscosity, density, and expansivity (see, for example, Takahashi, 1978; Watson, 1977; Mysen and Virgo, 1980; Dingwell and Virgo, 1987; Dingwell et al., 1988; Bottinga et al., 1982, 1983; Bockris and Kojonen, 1960; Robinson, 1969; Hofmann and Magaritz, 1977; Bockris and Reddy, 1970)—will, therefore, also vary with $Fe^{3+}/\Sigma Fe$ of the melt.

In Fe-bearing aluminosilicate systems, crystal-liquid phase equilibria and other properties also depend on the abundance of Al^{3+} and on the types of cations that charge-balance Al^{3+} and Fe^{3+} in tetrahedral coordination (Muan and Osborn, 1965; Riebling, 1964, 1966; Navrotsky et al., 1982; Seifert et al., 1982a). It has been suggested that the stabilities of aluminosilicate liquidus minerals (e.g., feldspars) depend on the proportion of related structural units in the melts (e.g., Burnham, 1981; Fraser et al., 1983; Mysen et al., 1982a). If so, the liquidus fields of such minerals depend, therefore, on the $Fe^{3+}/\Sigma Fe$ of the liquid whether or not appreciable amounts of iron oxides

0003–004X/89/0102–0058$02.00

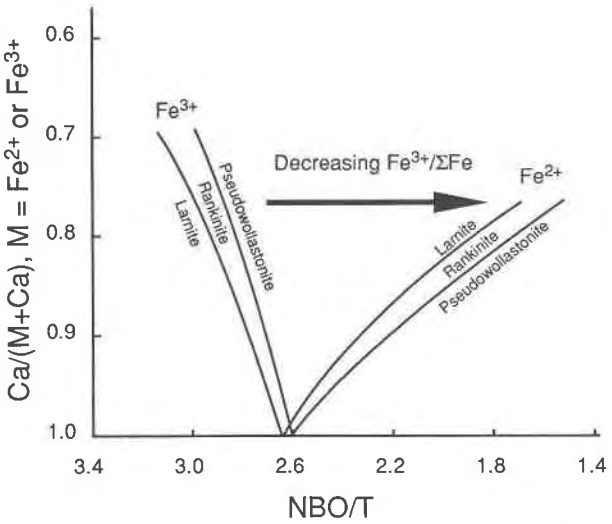

Fig. 1. Shifts of liquidus boundaries (expressed as degree of polymerization of the melt with the assumption of tetrahedrally coordinated Fe^{3+} and octahedrally coordinated Fe^{2+}) indicated in the systems CaO-FeO-SiO_2 and CaO-Fe_2O_3-SiO_2 (phase-equilibrium data from Osborn and Muan, 1960a, 1960b).

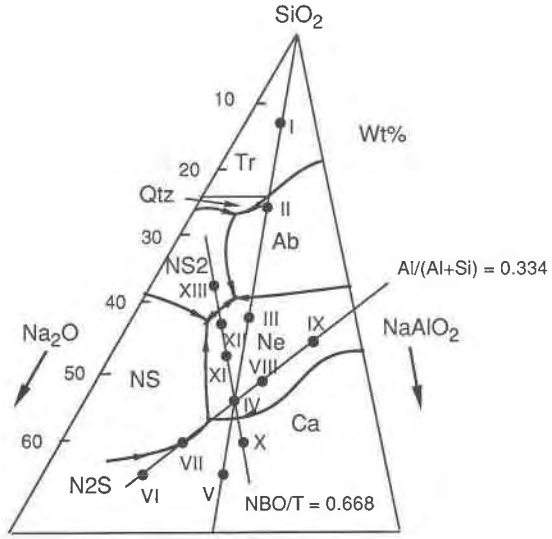

Fig. 2. Composition of starting materials (Fe-free; designated in text by NAS plus roman numeral; see Table 1) and the principal liquidus-phase equilibria in the relevant portions of the system Na_2O-Al_2O_3-SiO_2 (Osborn and Muan, 1960c). Abbreviations: NS, Na_2SiO_3; NS2, $Na_2Si_2O_5$; N2S, Na_4SiO_4; Tr, tridymite; Qtz, quartz; Ne, nepheline; Ca, carnegieite.

are contained in the mineral(s). Furthermore, because lowering of $Fe^{3+}/\Sigma Fe$ can result in depolymerization of the liquid, the liquidus phase of a silicate liquid may change to a more depolymerized mineral (e.g., pyroxene to olivine) as the $Fe^{3+}/\Sigma Fe$ ratio is decreased. In other words, decreasing $Fe^{3+}/\Sigma Fe$ (with constant total iron oxide content) is equivalent to increasing the concentration of network-modifying cations (in this case Fe^{2+}), thus possibly affecting liquidus phase equilibria, as also discussed by Kushiro (1975) and Ryerson (1985). This principle is illustrated in Figure 1 (data from Osborn and Muan, 1960a, 1960b). In this figure, the degree of polymerization (NBO/T) along liquidus boundaries of iron-free calcium silicate minerals with different degrees of polymerization (pseudowollastonite, rankinite, and larnite have NBO/Si equal to 2, 3, and 4, respectively) is shown as a function of $Ca/(Ca + Fe^{2+})$ (curve marked Fe^{3+}) and $Ca/(Ca + Fe^{3+})$ (curve marked Fe^{3+}). The arrow indicates the direction of shift of these liquidus boundaries as a function of decreasing $Fe^{3+}/\Sigma Fe$ for constant total Fe content. Clearly, from these phase-relationship data, the liquidus field of the least-polymerized phase expands with decreasing $Fe^{3+}/\Sigma Fe$. Thus, the redox ratio of Fe in magmatic liquids will influence liquid fractionation trends even without precipitation of iron oxide(s) in the fractionation process (see Osborn, 1959, for consequences of iron oxide crystallization from basaltic magma).

In view of the above considerations, it was decided to undertake a study on the relationships among redox equilibria of Fe, melt structure, and properties in Na_2O-Al_2O_3-SiO_2-Fe-O melt. In combination with data already available in related alkali and alkaline-earth aluminosilicate melt systems, a basis for quantitative characterization of the role of redox equilibria in natural magmatic systems might be developed.

Experimental methods

The Fe-free compositions in the system Na_2O-Al_2O_3-SiO_2 (Fig. 2) were chosen so as to encompass the range of Al/(Al + Si) and NBO/T (Table 1) commonly encountered in igneous rocks (0.15–0.4 and 0.1–1.0, respectively; Mysen, 1987). This compositional range also covers liquidus boundaries of minerals with greatly different compositions and degrees of polymerization (Osborn and Muan, 1960c; see also Fig. 2).

The starting materials were produced by grinding mixtures of spectroscopically pure Na_2CO_3, Al_2O_3, and SiO_2 (Johnson and Matthey, Inc.) under alcohol in batches of 250 mg for approximately 1 h. This material was decarbonated near 800 °C for 2 h, and the temperatures were slowly raised to immediately above that of the liquidus to produce the Fe-free base glass. Iron oxide

Table 1. Nominal composition of starting materials

	NASI	NASII	NASIII	NASIV	NASV	NASVI	NAS-VII
SiO_2	78.97	71.08	55.54	43.97	33.75	35.06	39.42
Al_2O_3	5.63	8.42	13.89	18.70	21.56	14.89	16.77
Na_2O	10.39	15.50	25.58	32.33	39.69	45.05	38.82
Fe_2O_3	5.00	5.00	5.00	5.00	5.00	5.00	5.00

	NAS-VIII	NASIX	NASX	NASXI	NAS-XII	NAS-XIII
SiO_2	47.32	52.43	37.61	49.63	53.63	58.69
Al_2O_3	20.12	22.30	21.89	14.30	11.37	7.97
Na_2O	27.56	20.27	35.50	31.34	30.00	28.35
Fe_2O_3	5.00	5.00	5.00	5.00	5.00	5.00

TABLE 2. Experimental results

Composition	T (°C)	log f_{O_2}*	Fe^{3+}		Fe^{2+}(I)		Fe^{2+}(II)		$Fe^{3+}/\Sigma Fe$
			IS	QS	IS	QS	IS	QS	
NASI	1550	−0.68	0.29	0.90	0.91	2.05	—	—	0.797
NASII	1550	−0.68	0.29	0.88	0.93	2.10	—	—	0.730
NASII**	1550	−0.68	0.38	0.94	1.14	2.40	0.96	2.04	0.754
NASIII	1550	−0.68	0.29	0.87	0.88	2.12	—	—	0.745
NASIV	1550	−0.68	0.25	0.94	0.90	2.11	—	—	0.790
NASV	1550	−0.68	0.23	1.07	0.94	1.89	—	—	0.799
NASVI	1550	−0.68	0.23	0.95	0.97	1.99	—	—	0.843
NASVII	1550	−0.68	0.24	0.96	0.88	2.15	—	—	0.827
NASVIII	1550	−0.68	0.23	0.99	0.94	1.95	—	—	0.743
NASIX	1550	−0.68	0.26	0.97	0.91	1.97	—	—	0.779
NASX	1550	−0.68	0.23	0.98	0.88	2.10	—	—	0.816
NASXI	1550	−0.68	0.26	0.91	0.91	2.08	—	—	0.763
NASXII	1550	−0.68	0.27	0.87	0.91	2.15	—	—	0.748
NASXIII	1550	−0.68	0.27	0.87	0.99	2.24	—	—	0.761
NASIV	1400	−0.68	0.22	0.98	0.94	1.97	—	—	0.858
NASVII	1400	−0.68	0.23	0.93	0.77	2.29	—	—	0.871
NASVIII	1400	−0.68	0.25	0.97	0.87	2.21	—	—	0.848
NASIX	1400	−0.68	0.23	0.98	0.82	2.07	—	—	0.862
NASXIII	1400	−0.68	0.27	0.86	0.91	2.14	—	—	0.823
NASIV	1250	−0.68	0.24	0.98	0.75	2.18	—	—	0.918
NASIX	1250	−0.68	0.23	0.99	0.61	2.02	—	—	0.893
NASXIII	1250	−0.68	0.26	0.91	0.88	2.08	—	—	0.895
NASIV	1550	−2.00	0.28	0.82	0.90	2.32	0.72	1.95	0.683
NASIV**	1550	−2.00	0.36	0.95	1.02	2.44	1.08	1.98	0.676
NASIV	1550	−3.00	0.44	0.60	0.97	2.31	0.79	1.96	0.472
NASIV**	1550	−3.00	0.45	0.77	1.11	2.44	1.11	2.07	0.487
NASIX	1550	−3.00	0.52	0.50	0.94	2.10	0.73	1.67	0.355
NASXIII	1550	−3.00	0.48	0.56	1.03	2.28	0.87	1.95	0.340
NASIV	1400	−3.00	0.21	0.98	0.98	1.88	—	—	0.655
NASVIII	1400	−3.00	0.26	0.93	1.01	2.16	0.87	1.87	0.749
NASIV	1250	−3.00	0.28	0.90	0.80	2.24	—	—	0.811
NASIX	1250	−3.00	0.26	0.92	0.82	2.20	—	—	0.815
NASXIII	1250	−3.00	0.29	0.93	1.02	2.28	0.85	1.93	0.800
NASIV	1550	−4.50	0.54	0.54	0.96	2.24	0.92	1.74	0.297
NASIV**	1550	−4.50	0.60	0.68	1.10	2.46	1.05	1.86	0.256
NASIV	1550	−6.00	0.59	0.70	0.99	2.17	0.98	1.61	0.200
NASIV**	1550	−6.00	0.83	0.67	1.12	2.37	1.08	1.75	0.184
NASIX	1550	−6.00	0.75	0.75	1.07	1.93	0.88	1.56	0.101
NASXIII	1550	−6.00	0.57	0.33	1.00	2.23	0.97	1.72	0.087
NASXIII**	1550	−6.00	0.62	0.38	1.08	2.24	0.97	1.73	0.136
NASIV	1400	−6.00	0.35	0.66	0.96	2.25	0.81	1.95	0.475
NASIV	1250	−6.00	0.28	0.85	0.93	2.03	—	—	0.572
NASIX	1250	−6.00	0.27	0.88	1.01	2.11	0.85	1.80	0.628
NASXIII	1250	−6.00	0.36	0.73	1.04	2.08	0.79	1.89	0.444
NASIV	1400	−7.50	0.59	0.47	0.98	2.22	0.94	1.69	0.188
NASIV	1550	−9.00	—	—	1.19	2.39	1.12	1.60	0.000
NASIV**	1550	−9.00	—	—	1.21	2.45	1.15	1.71	0.000
NASIX	1550	−9.00	—	—	1.21	2.45	1.15	1.71	0.000
NASXIII	1550	−9.00	—	—	1.01	2.11	0.98	1.58	0.000
NASIV	1400	−9.00	0.70	0.58	0.97	2.22	0.94	1.56	0.121
NASIV	1250	−9.00	0.56	0.40	0.97	2.25	0.91	1.72	0.234
NASIX	1250	−9.00	0.50	0.45	0.91	2.16	0.86	1.59	0.395
NASXIII	1250	−9.00	0.59	0.32	0.99	2.24	0.95	1.71	0.200

Note: IS and QS (isomer shift and quadrupole splitting, mm/s) relative to Fe^0.
* f_{O_2} in bars.
** Spectrum obtained at 77 K.

was added (in this study, 5 wt% Fe_2O_3 was added to all starting compositions) as spectroscopically pure Fe_2O_3 with approximately 10% $^{57}Fe_2O_3$ enrichment to facilitate Mössbauer analysis. Quenched, Fe-bearing melts were formed by suspending sintered 50- to 80-mg pellets of starting materials on 0.1-mm-diameter Pt loops (Presnall and Brenner, 1974) in vertical quench furnaces (Pt- and $MoSi_2$-heated). The weight ratio of sample to Pt was approximately 100/1. Mysen and Virgo (1978), in their study of melts on the composition join $NaAlSi_2O_6$-$NaFe^{3+}Si_2O_6$ with similar sample size and configuration, found from time studies that 30 min was sufficient time to obtain redox ratios that did not change with additional run duration, and 30- to 90-min experimental run durations were employed in the present study. The run durations were kept this short in order to minimize possible Fe loss to the Pt loop and alkali loss to the atmosphere. Reliable electron-microprobe analyses of the quenched glasses could not be obtained because of Na volatilization under the microprobe beam. In experiments with equivalent Ca- and Mg-bearing melts, however, Mysen et al. (1985a) found 5–10% Fe loss under these conditions. Similar uncertainties probably apply, therefore, to the present samples.

The oxygen fugacity in the furnace was controlled with CO-CO_2 gas mixing with an yttria-doped ZrO_2 oxygen-fugacity sensor (Sato, 1972) to monitor the f_{O_2}. The oxygen fugacity was

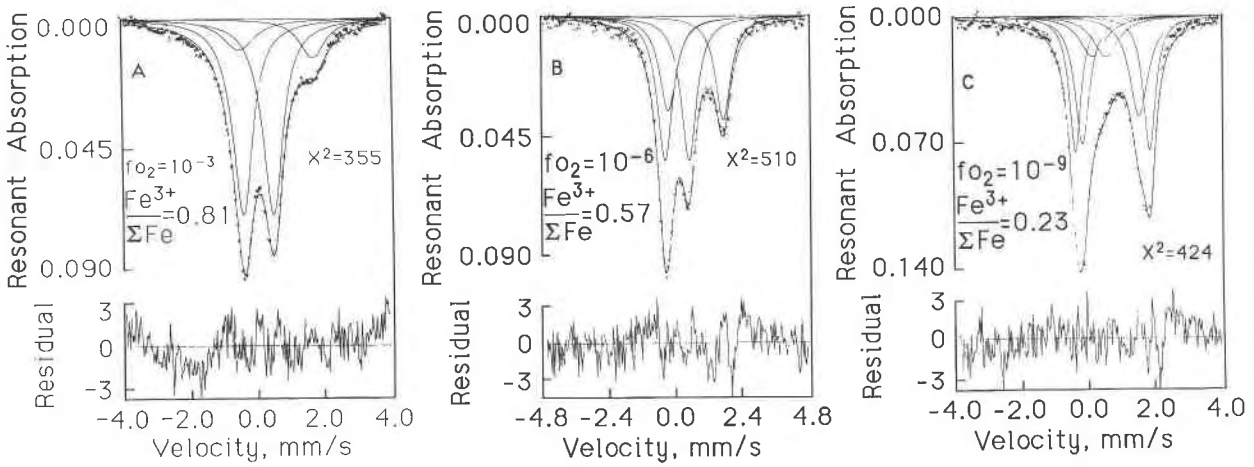

Fig. 3. ^{57}Fe resonant–absorption Mössbauer spectra (at 298 K) of quenched NASIVF5 melts as a function of oxygen fugacity at 1250 °C.

precise to within 0.01–0.02 log units and accurate to better than 0.1 log unit as calibrated against Ni-NiO and Fe-FeO oxide buffers (Chou, 1978; Deines et al., 1974). The temperatures were monitored with one S-type ($Pt\text{-}Pt_{90}Rh_{10}$) thermocouple (calibrated against the melting point of Au) 1 cm above the sample and another S-type thermocouple inside the oxygen-fugacity sensor displaced approximately 1 cm horizontally from the sample. The temperatures recorded with these thermocouples differed by less than 2 °C. The experiments were terminated by quenching on a Pt disc standing in liquid N_2 or quenched directly in water. The quenching rates were on the order of 500 °C/s to temperatures less than 1000 °C resulting in glasses free of quench crystals. These quenching rates are comparable to the most rapid quenching rates in the rate studies by Dyar and coworkers (e.g., Dyar and Birnie, 1984; Dyar et al., 1987) where only "subtle" changes in the Mössbauer spectra were observed. Those investigators worked with highly depolymerized lunar basalt glasses (NBO/T $\approx$ 1.8). Most likely, because of the highly depolymerized nature of these materials compared with those of the present study (Table 1), their lunar basalt melts were probably more fluid and, thus, more susceptible to changes during quenching. Even so, with the highest quenching rates in their studies, little effect of quenching rates was observed, and it seems likely that similar conclusions apply to the more viscous melts used here. Furthermore, although structural studies of Fe-bearing melts in their molten state have not been carried out, it is worth noting that from vibrational spectral data of melts and glasses in the Fe-free $Na_2O\text{-}Al_2O_3\text{-}SiO_2$ system (e.g., Sweet and White, 1969; Sharma et al., 1978; Seifert et al., 1981), it was concluded that structural changes within the sensitivities of the methods could not be discerned. These observations further support the conclusion that the reported $Fe^{3+}/\Sigma Fe$ and types of oxygen coordination polyhedra are the same in the melts as in the quenched melts (glasses). This conclusion does not rule out, however, possible effects caused by slower quenching rates for lunar glasses as suggested, for example, by Dyar and Birnie (1984).

Redox ratios of Fe and information on the structural positions of Fe^{3+} and Fe^{2+} in the glasses were obtained with Mössbauer spectroscopy using the methods described by Mysen et al. (1980, 1985b) and Virgo and Mysen (1985). The spectra were fitted statistically with Lorentzian lines by using the same computational and statistical methods as described by Seifert et al. (1982a) and Mysen et al. (1982b, 1985b). This fitting procedure was found satisfactory for spectra of Fe-bearing aluminosilicate melts (Virgo et al., 1983a; see also Virgo et al., 1983b, and Virgo and Mysen, 1985, for comparison of structural interpretations based on these and other fitting routines and interpretations based on, and compared with, optical and Raman spectroscopy). In these spectra, at least one Fe^{3+} and one Fe^{2+} doublet were included. For each Fe^{2+} doublet, the integrated areas of the constituent peaks were constrained to be equal. For the Fe^{3+} quadrupole-splitting doublets, both area and half width were constrained to be equal. A detailed discussion of the rationale behind these constraints and a comparison of the results obtained with this fitting method and others were provided by Virgo and Mysen (1985). In the samples formed with f_{O_2} less than that of air (lower $Fe^{3+}/\Sigma Fe$), statistical considerations (χ^2 and distribution of residuals) sometimes indicated two Fe^{2+} doublets in the high-velocity portion of the absorption envelope. The velocity difference between the two low-velocity components of these Fe^{2+} doublets commonly was so small (<0.1 mm/s) that, for oxidized samples, the deconvolution procedure generally caused a merger of the two low-velocity components in all but the most reduced samples. The $Fe^{3+}/\Sigma Fe$ of the samples was obtained from the Mössbauer spectra as the ratio of the area of the Fe^{3+} doublet relative to the total absorption envelope. A comparison of $Fe^{3+}/\Sigma Fe$ from 28 experimentally produced glasses obtained with this method with determination of $Fe^{3+}/\Sigma Fe$ of the same samples with a wide range of $Fe^{3+}/\Sigma Fe$, total Fe content, and bulk composition from wet-chemical determination (Mysen et al., 1985b) demonstrated that the $Fe^{3+}/\Sigma Fe$ from either method was equally reliable. Similar conclusions were reached by Dyar et al. (1987).

Results

Mössbauer spectra

Experimental results on redox ratios of Fe and calculated hyperfine parameters (quadrupole splitting, QS, and isomer shift, IS) are given in Table 2. Representative ^{57}Fe resonant–absorption Mössbauer spectra (Figs. 3–5) are included to illustrate the spectroscopic changes in sam-

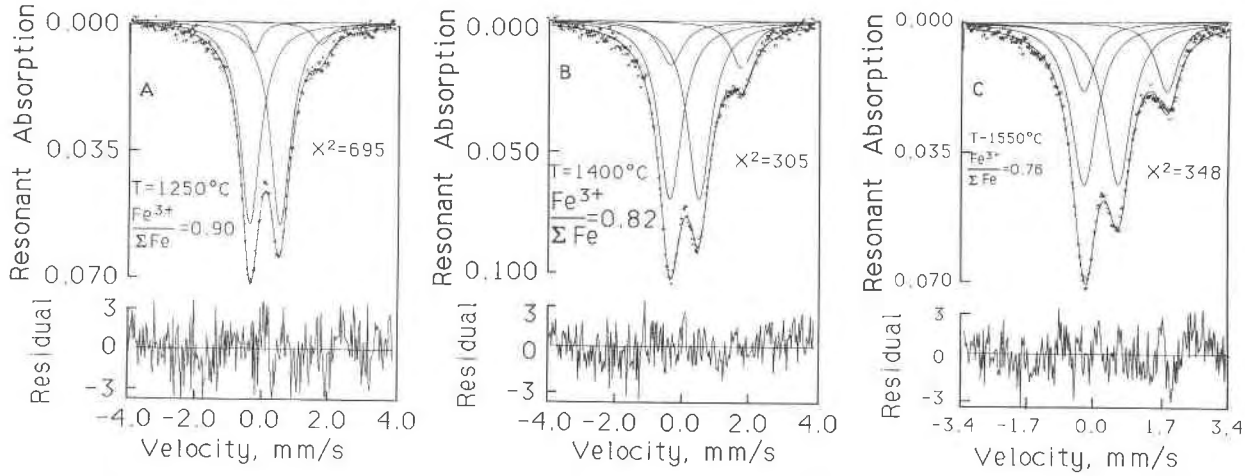

Fig. 4. ^{57}Fe resonant–absorption Mössbauer spectra (at 298 K) of quenched NASIVF5 melts as a function of temperature at the oxygen fugacity of air.

ples with variations in oxygen fugacity (Fig. 3), temperature (Fig. 4), Al/(Al + Si), and degree of polymerization (NBO/T) (Fig. 5).

The topological evolution of the spectra as a function of decreasing oxygen fugacity and increasing temperature is qualitatively similar for all compositions. Increasing temperature (at constant oxygen fugacity) or decreasing oxygen fugacity (at constant temperature) results in increased absorption near 1.8 mm/s (high-velocity components of Fe^{2+} doublet) and decreased absorption near 0.5 mm/s (high-velocity component of Fe^{3+} doublet).

All the 298-K spectra of samples equilibrated with air (see Table 2 and also Figs. 4 and 5) are deconvoluted into one Fe^{3+} and one Fe^{2+} doublet. From these spectra, the average isomer shifts of Fe^{3+} and Fe^{2+} (relative to Fe^0) are 0.25 ± 0.02 and 0.92 ± 0.08 mm/s, respectively. Generally, the $IS_{Fe^{2+}}$ and $IS_{Fe^{3+}}$ values from 77-K spectra are about 0.1 mm/s higher than those obtained at 298 K (Table 2). The quadrupole splittings for Fe^{3+} and Fe^{2+} doublets are 0.94 ± 0.05 mm/s and 2.09 ± 0.10 mm/s, respectively. The 77-K spectrum of sample NASII (see Fig. 2 and Table 1 for composition) is better resolved than the 298-K spectrum, and two Fe^{2+} doublets result in a better fit to the cumulative envelope than one Fe^{2+} doublet. For spectra of samples equilibrated at f_{O_2} less than that of air, the $Fe^{3+}/\Sigma Fe$ is lower, and commonly two Fe^{2+} doublets are inserted rather than one. Two Fe^{2+} doublets in Fe^{2+}-rich samples have also been fitted to spectra of hydrous granite composition (Spiering and Seifert, 1985) and in spectra of lunar-composition glass (e.g., Dyar and Birnie, 1984; Dyar et al., 1987). Among these two doublets, the one denoted Fe^{2+}(I) (see Table 2) has an average isomer shift (IS) value of 0.99 ± 0.09 mm/s, whereas the other doublet, denoted Fe^{2+}(II), has IS = 0.91 ± 0.11 mm/s. These values do, however, tend to increase with decreasing $Fe^{3+}/\Sigma Fe$ and are near 1.1 mm/s in Fe^{3+}-free glass (Table 2; see also Virgo and Mysen, 1985). Whether this shift reflects real changes of the Fe^{2+}-O coordination polyhedra as a function of $Fe^{3+}/\Sigma Fe$ in the glass or represents statistical limitations in the deconvolution procedure cannot be ascertained.

In the highly oxidized samples, the low-velocity components of the Fe^{3+} and Fe^{2+} doublets nearly coincide. This conclusion is in accord with the assumption by Mysen and Virgo (1978) and Mysen et al. (1980) in their three-line fits of spectra in iron-bearing sodium silicate and sodium aluminosilicate glasses. The fits differ, however, from spectra of iron-bearing calcium and magnesium silicate glasses, where the low-velocity component of the Fe^{3+} doublet typically occurs at 0.1-mm/s lower velocity than that of the low-velocity component of Fe^{2+} doublet. Larger values of $QS_{Fe^{3+}}$ for the alkaline-earth silicate glasses were, thus, obtained (see also Virgo et al., 1983a; Mysen et al., 1984, 1985a). The Mössbauer spectra from Fe^{3+}-rich samples in alkali and alkaline-earth silicate systems also differ in that in the alkali silicate systems, the line widths (full width at half height, FWHH) typically are on the order of 0.6 to 0.7 mm/s, whereas in the alkaline-earth systems, the FWHH line widths range from 0.8 to 1.0 mm/s.

The spectral region near 0.5 mm/s rapidly loses structure with decreasing oxygen fugacity. The diminished absorption near 0.5 mm/s results from a broadening of the component peaks of the Fe^{3+} doublet (from about 0.6 mm/s half width at half height in the most oxidized samples to about 0.8–0.9 mm/s in the reduced samples). There is also a gradual shift of the position of the low-velocity component from near −0.3 mm/s to near 0 mm/s with decreasing f_{O_2} (see Fig. 3). The velocity of the high-velocity component of the Fe^{3+} doublet has increased by about 0.1 mm/s in these spectra compared with the velocity of the high-velocity component of the Fe^{3+} doublet in oxidized samples. A similar spectral trend with decreasing $Fe^{3+}/\Sigma Fe$ was observed in the spectra of alkaline-earth silicate and aluminosilicate samples (Virgo et al., 1983a; Mysen et al., 1984, 1985a). The latter spectra differ some-

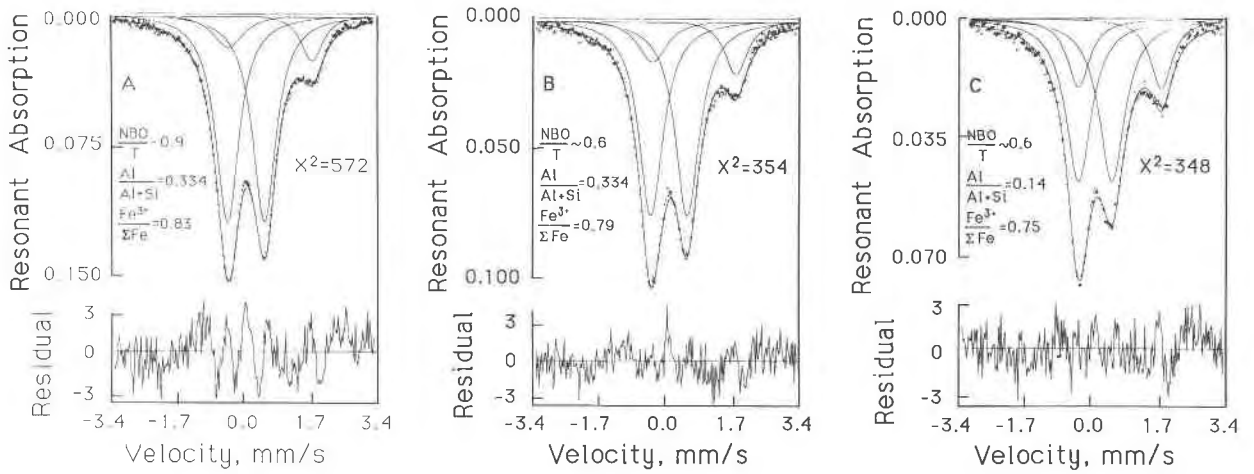

Fig. 5. ^{57}Fe resonant–absorption Mössbauer spectra of NASVIIF5 (**A**), NASIVF5 (**B**), and NASXIIF5 (**C**) composition quenched melts equilibrated with air at 1550 °C.

what, however, from those of sodium aluminosilicate glasses in that the high-velocity component of the Fe^{3+} doublet shifts from about 0.5 mm/s to values near 0.8–0.9 mm/s with decreasing $Fe^{3+}/\Sigma Fe$, whereas the maximum value in the sodium aluminosilicate system is near 0.65 mm/s for spectra obtained at 298 K. In the 77-K spectra, the high-velocity components of the Fe^{2+} and Fe^{3+} doublets occur at values about 0.1–0.15 mm/s higher than in the 298-K spectra, thus giving rise to the changes in QS and IS values shown in Table 2.

The isomer shifts and quadrupole splittings of Fe^{3+} in the aluminosilicate glasses are systematic functions of the $Fe^{3+}/\Sigma Fe$ in the $Fe^{3+}/\Sigma Fe$ range between 0.6 and 0.3 (Fig. 6). The $IS_{Fe^{3+}}$ increases rapidly from 0.3 mm/s for glasses with $Fe^{3+}/\Sigma Fe > 0.6$ to values between 0.5 and 0.6 mm/s with $Fe^{3+}/\Sigma Fe < 0.3$. This change is associated with a decrease of $QS_{Fe^{3+}}$ from an average near 0.9–1.0 mm/s for oxidized samples to near 0.4 mm/s with $Fe^{3+}/\Sigma Fe < 0.3$. In the intermediate $Fe^{3+}/\Sigma Fe$ range (0.6–0.3), the $IS_{Fe^{3+}}$ and $QS_{Fe^{3+}}$, whether from 298-K or 77-K spectra, exhibit intermediate values (Table 2, Fig. 6). These relationships between $Fe^{3+}/\Sigma Fe$ and hyperfine parameters are independent of temperature, oxygen fugacity, and bulk composition, although they are tied to these parameters insofar as their control of the $Fe^{3+}/\Sigma Fe$ itself is concerned. Similar relationships have been reported for other systems and other temperatures, pressures, and oxygen-fugacity values (Mysen et al., 1984, 1985a; Virgo and Mysen, 1985; Mysen and Virgo, 1985). Virgo and Mysen (1985) were able to insert two Fe^{3+} doublets in some of the spectra from samples in the system Na_2O-Al_2O_3-SiO_2-Fe-O in this $Fe^{3+}/\Sigma Fe$ range. In those fits, the velocities of the component peaks of the two Fe^{3+} doublets were similar to those for the oxidized and reduced samples, respectively. When fitted in this fashion, the isomer-shift and quadrupole-splitting values for the two Fe^{3+} doublets did not change as a function of $Fe^{3+}/\Sigma Fe$, but their relative intensities were systematic functions of $Fe^{3+}/\Sigma Fe$.

Structural interpretations of the spectra

The hyperfine parameters (isomer shifts and quadrupole splitting) of Fe^{2+} and Fe^{3+} are sensitive to structure. In particular, the isomer shift of Fe^{3+} ($IS_{Fe^{3+}}$) and, to a lesser degree, the quadrupole splitting ($QS_{Fe^{3+}}$) respond to

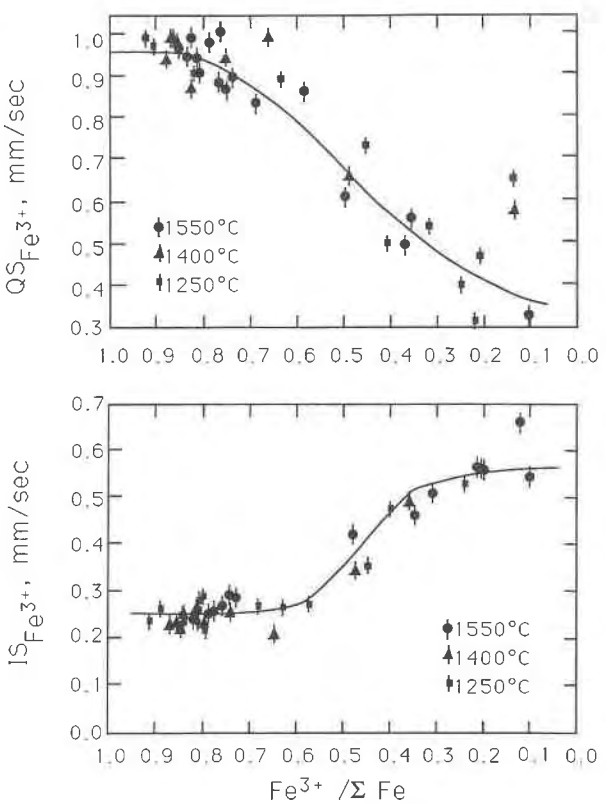

Fig. 6. Relations between isomer shift ($IS_{Fe^{3+}}$) and quadrupole splitting ($QS_{Fe^{3+}}$) of Fe^{3+} (mm/s, relative to Fe^0) as a function of $Fe^{3+}/\Sigma Fe$.

the number of oxygen ligands in and the distortion of the polyhedra.

Ferric iron. Information from crystalline silicates aids in the interpretation of the spectra of Fe-bearing glasses. In crystalline iron silicates, 298-K values of $IS_{Fe^{3+}} < 0.3$ mm/s (relative to Fe^0) typically result from tetrahedrally coordinated Fe^{3+}, whereas values greater than about 0.5 mm/s are due to octahedrally coordinated Fe^{3+} (Annersten and Olesch, 1978; Seifert et al., 1979; Mysen et al., 1980; Virgo et al., 1981, 1983a; Calas and Petiau, 1983a, 1983b; Waychunas and Rossman, 1983). The isomer shift of Fe^{3+} in oxidized glass samples ($Fe^{3+}/\Sigma Fe > 0.6$) is near 0.26 mm/s and 0.35 mm/s at 298 K and 77 K, respectively. This temperature-dependence of the $IS_{Fe^{3+}}$ compares well with that observed for tetrahedrally coordinated Fe^{3+} of crystalline silicates [about 5×10^{-4} mm/(s·K); see Hafner and Huckenholz, 1971; Amthauer et al., 1977].

The assignment of Fe^{3+} to tetrahedral coordination in oxidized glasses is also supported by results from other spectroscopic techniques. The *K*-edge X-ray absorption spectrum of $Na_2O \cdot 2SiO_2$ glass, containing 3 wt% Fe_2O_3 equilibrated with air at 1200 °C, was studied by Calas and Petiau (1983a, 1983b). Those investigators concluded that the minimum proportion of tetrahedrally coordinated Fe^{3+} was 70%. Furthermore, Raman spectra of Fe-bearing glasses on the join Na_2O-SiO_2 (Fox et al., 1982; Virgo et al., 1983a), formed by melting in the temperature range 1250–1550 °C in equilibrium with air, indicated that $^{[4]}Fe$–O bonds existed in the samples. The assignment by Fox et al. (1982) was further supported by luminescence spectra. From this comparison of Mössbauer spectra of crystalline and glassy materials, as well as data from other spectroscopic techniques, it is concluded that for $IS_{Fe^{3+}} < 0.3$ mm/s, Fe^{3+} is tetrahedrally coordinated in the glass.

The $QS_{Fe^{3+}}$ may be considered a measure of the degree of distortion of the Fe^{3+}-O polyhedra. For example, from the trends of $QS_{Fe^{3+}}$ in crystalline ferrisilicate minerals with tetrahedral Fe^{3+} (e.g., Annersten, 1976; Hafner and Huckenholz, 1971; Glasser et al., 1972), it has been found that the quadrupole splitting of Fe^{3+} increases from 0.0 in an ideal cubic symmetry to values near 0.5–0.6 in $KFe^{3+}Si_3O_8$ and about 1.5 mm/s in $CaFeSi^{3+}Si_2O_6$, where the FeO_2 tetrahedra are highly distorted. For the present glasses, the average room-temperature (298-K) quadrupole splitting of $^{[4]}Fe^{3+}$ is 0.93 ± 0.05 mm/s (31 samples with $IS_{Fe^{3+}} < 0.3$ mm/s) suggesting, therefore, significant distortion of the polyhedron. In comparison, in the equivalent CaO-Al_2O_3-SiO_2 and MgO-Al_2O_3-SiO_2 glass systems, the average quadrupole splittings were 1.31 ± 0.07 mm/s (30 samples) and 1.43 ± 0.06 mm/s (6 samples) (Mysen et al., 1985a). This trend of increasing $QS_{Fe^{3+}}$ with increasing Z/r^2 of the metal cation might be the result of increasing distortion of the Fe^{3+}-bearing tetrahedra as the Z/r^2 of the charge-balancing cations increases. In reduced samples ($Fe^{3+}/\Sigma Fe < 0.3$), the isomer shifts for Fe^{3+} exceed 0.5 mm/s for 298-K spectra with values about 0.1 mm/s higher for 77-K spectra (Table 2, Fig. 6). The $IS_{Fe^{3+}}$ values from spectra of reduced samples are somewhat greater than those observed for octahedrally coordinated Fe^{3+} in crystalline silicates (Annersten et al., 1978; Hafner and Huckenholz, 1971; Amthauer et al., 1980; Evans and Amthauer, 1980; Nolet and Burns, 1979; Huggins et al., 1977), and assignments alternative to octahedrally coordinated Fe^{3+} might be entertained. It is possible, for example, that these higher $IS_{Fe^{3+}}$ values from the glassy materials compared with the $IS_{Fe^{3+}}$ from $^{[6]}Fe^{3+}$ in crystalline materials might reflect an intermediate oxidation state of Fe where an averaged electronic state between that of octahedrally coordinated Fe^{3+} and octahedrally coordinated Fe^{2+} might be recorded (electron hopping). From crystalline oxides and silicates, two extreme cases of electron hopping may be considered: (1) The exchange electrons are localized on neighboring sites in the lattice, or (2) the electrons are delocalized over the whole sublattice. Delocalized hopping has been observed above the Verwey transition in Fe_3O_4 spinel (Weber and Hafner, 1971; Haggstrom et al., 1978) and localized electron hopping in spinels and silicates (e.g., Grandjean and Gerard, 1978; Annersten and Hafner, 1973; Evans and Amthauer, 1980; Coey et al., 1982). For the glasses, localized electron hopping is unlikely, however, because the intensity of the Fe^{3+} absorption is insensitive to the temperature at which the spectra were recorded (Table 2). Delocalized electron hopping between octahedral Fe^{3+} and octahedral Fe^{2+} locations in the glass is possible. It is suggested that this process may take place in the reduced glasses, where Fe^{3+} is in octahedral coordination. Similar conclusions might apply to the interpretation of the Mössbauer spectra of other alkali and alkaline-earth silicate and aluminosilicate glasses (see also Virgo and Mysen, 1985, for a more detailed description and discussion of such processes).

In the $Fe^{3+}/\Sigma Fe$ range between 0.6 and 0.3, the $IS_{Fe^{3+}}$ increases gradually with decreasing $Fe^{3+}/\Sigma Fe$. Whether this change reflects a gradual shift of an individual doublet or whether there is more than one Fe^{3+} doublet in the spectra of these glasses cannot be resolved statistically. It is suggested, however, that the observed gradual changes in $IS_{Fe^{3+}}$ and $QS_{Fe^{3+}}$ in the $Fe^{3+}/\Sigma Fe = 0.6$–0.3 range reflect a gradual coordination transformation of Fe^{3+} from tetrahedral to octahedral coordination.

In correlative studies utilizing Mössbauer and Raman spectroscopy, Virgo et al. (1983b) and Mysen et al. (1985a) found that the $Fe^{3+}/\Sigma Fe$–dependent changes of the hyperfine parameters were also associated with a rapidly diminishing intensity of Raman bands from $^{[4]}Fe^{3+}$–O bonds in alkali and alkaline-earth silicate melts. In those spectra, the intensities of the $^{[4]}Fe^{3+}$–O stretch bands near 900 and 980 cm^{-1} diminished rapidly with decreasing $Fe^{3+}/\Sigma Fe$ in the $Fe^{3+}/\Sigma Fe$ range between ~0.5 and ~0.3. Neither the 900- nor the 980-cm^{-1} band could be observed in the Raman spectra of glasses with $Fe^{3+}/\Sigma Fe <$

0.3 (Virgo et al., 1983b; Mysen et al., 1985a). Those data further substantiate, therefore, the interpretation of the Mössbauer hyperfine parameters.

From the discussion of the isomer-shift variations above, it is concluded that Fe^{3+} is in tetrahedral coordination in silicate glasses with $Fe^{3+}/\Sigma Fe > 0.6$ and in octahedral coordination with $Fe^{3+}/\Sigma Fe < 0.3$. An intermediate $Fe^{3+}/\Sigma Fe$ range exists (0.6–0.3) where tetrahedral Fe^{3+} and octahedral Fe^{3+} coexist in the melts. Similar conclusions, based on similar kinds of spectroscopic data (Mössbauer and Raman spectroscopy) were reached for melts in the systems CaO-Al_2O_3-SiO_2-Fe-O and MgO-Al_2O_3-SiO_2-Fe-O (Mysen et al., 1985a). This type of structural interpretation has also been employed to rationalize viscosity and volumetric data in the system Na_2O-FeO-Fe_2O_3-SiO_2 (Dingwell and Virgo, 1987; Dingwell et al., 1988).

The coordination transformation of Fe^{3+} is governed by the value of the $Fe^{3+}/\Sigma Fe$ and is, therefore, also a function of any variable (intensive or extensive) that affects the $Fe^{3+}/\Sigma Fe$. Interestingly, for certain oxygen fugacities, Fe^{3+} may undergo a coordination transformation with increasing temperature. For example, at $f_{O_2} = 10^{-6}$ bar, melt of NASIVF5 composition [Al/(Al + Si) = 0.334, NBO/T $\approx$ 0.6, 5 wt% iron oxide added] has $IS_{Fe^{3+}} = 0.27$ mm/s at 1250 °C, 0.35 mm/s at 1400 °C, and 0.59 mm/s at 1550 °C (Table 2). Thus, Fe^{3+} is in fourfold coordination at 1250 °C and, most probably, in sixfold coordination at 1550 °C. At 1400 °C, the intermediate value of $IS_{Fe^{3+}}$ may result from a mixture of tetrahedral and octahedral Fe^{3+} in the melt.

Ferrous iron. From the results of the least-squares fitting of the absorption spectra (Table 2; Figs. 3–5), the statistical parameters often indicate an improved fit when two Fe^{2+} doublets are fitted to the spectra, observations also made in the Mössbauer spectra of glasses in more complex systems (Spiering and Seifert, 1985; Dyar et al., 1987). The values of the hyperfine parameters for a single Fe^{2+} doublet represent the average values of the two doublets. It is not clear, however, whether this inclusion of a second doublet has a structural interpretation or simply reflects an improved fit to the distribution of the hyperfine fields. Furthermore, it might be suggested that because the difference in the hyperfine-parameter values is quite small (typically less than 0.1 mm/s), the difference might be viewed as within the uncertainty.

Whether one or two doublets are fitted, the $IS_{Fe^{2+}}$ values increase in general by 10–20% and the $QS_{Fe^{2+}}$ values decrease somewhat with decreasing $Fe^{3+}/\Sigma Fe$ (Table 2). The range in values is similar to that reported for Fe^{2+} in other glasses (e.g., Nolet et al., 1979; Mao et al., 1973; Calas and Petiau, 1983b; Seifert et al., 1979). Most of these values (with an average near 0.95 mm/s) are, however, intermediate between those attributable to Fe^{2+} in octahedral and tetrahedral coordination in crystals. Only in the completely reduced samples are the hyperfine parameters for Fe^{2+} wholly consistent with those of octahedrally coordinated Fe^{2+} in crystalline silicates. Thus, the Mössbauer spectra of mixed-valence samples cannot be interpreted uniquely in regard to the Fe^{2+} coordination state.

An assignment of the Fe^{2+} absorption doublet(s) in glasses predominantly to octahedral coordination might be justified, however, with the aid of results from other spectroscopic techniques. For example, the infrared absorption spectra of Fe-bearing Na_2O-SiO_2 glasses contain two bands, at 10000 and 5000 cm^{-1}, which Fox et al. (1982) attributed to octahedrally coordinated Fe^{2+}. Raman spectra of this and other glass compositions containing only Fe^{2+} (Fox et al., 1982; Virgo et al., 1983a; Mysen et al., 1985c) showed no evidence of tetrahedrally coordinated Fe^{2+}. Finally, optical absorption spectra of a range of simple synthetic and complex natural glass compositions (e.g., Nolet et al., 1979; Nolet, 1980; Mao et al., 1973; Goldman and Berg, 1980) indicate that at the very least, only a minor proportion of Fe^{2+} iron could be in tetrahedral coordination. Thus, it is concluded that, in general, Fe^{2+} is in octahedral coordination in silicate glasses although there might be exceptions to this rule (see, for example, Raman data of nominally Fe_2SiO_4 composition glass; Cooney et al., 1987).

Redox equilibria

Melt compositional relationships. The $Fe^{3+}/\Sigma Fe$ ratio of silicate melts generally increases with oxygen ion activity (Larson and Chipman, 1953; Douglas et al., 1965). The observed positive correlation between $Fe^{3+}/\Sigma Fe$ and NBO/T (at NBO/T > 0.4) of the melt (Fig. 7) is in accord with those data. With NBO/T < 0.4, the $Fe^{3+}/\Sigma Fe$ decreases, however, with decreasing NBO/T (Fig. 7). Similar reversals in the $Fe^{3+}/\Sigma Fe$ vs. NBO/T trends at low NBO/T were observed in the systems Na_2O-SiO_2-Fe-O, BaO-SiO_2-Fe-O, and K_2O-SiO_2-Fe-O (Virgo et al., 1981). Under more reducing conditions, where Fe^{3+} is predominantly in octahedral coordination, the limited data suggest that the $Fe^{3+}/\Sigma Fe$ may increase with decreasing NBO/T. The positive correlation between NBO/T and $Fe^{3+}/\Sigma Fe$ (Fig. 7) has also been observed in a number of other simple silicate systems (e.g., Larson and Chipman, 1953; Douglas et al., 1965; Holmquist, 1966; Virgo et al., 1981, 1983a; Mysen et al., 1984, 1985a).

The principal relationship can be illustrated with the expression (Holmquist, 1966)

$$4FeO_2^- \rightleftharpoons 4Fe^{2+} + O_2 + 6O^{2-}. \quad (1)$$

This equation can be integrated with anionic equilibria (Virgo et al., 1980; Furukawa et al., 1981; Mysen et al., 1982a; Matson et al., 1983) to illustrate the interaction between Fe and the melt structure. In its simplest form, such an equation is

$$4FeO_2^- + 12SiO_2 \rightleftharpoons 4Fe^{2+} + 6Si_2O_5^{2-} + O_2. \quad (2)$$

Thus, reduction of Fe^{3+} to Fe^{2+} is associated with depolymerization of the melt.

There is no evidence in the Mössbauer data (Table 2)

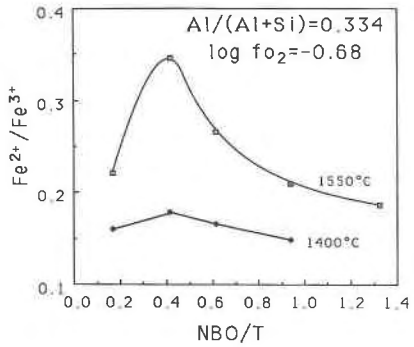

Fig. 7. Relationships between Fe^{2+}/Fe^{3+} and NBO/T as a function of temperature at $f_{O_2} = 10^{-0.68}$ bar.

or in the Mössbauer and Raman data reported by Virgo et al. (1981) for binary metal oxide–silica melts to indicate that the minimum $Fe^{3+}/\Sigma Fe$ near NBO/T = 0.4 (Fig. 7) is associated with a change of the coordination state of Fe^{3+} in the melts. One may speculate, however, that the transition results from increasing difficulty of Fe^{2+} to form $^{[6]}Fe^{2+}$-O polyhedra as the NBO/T decreases in these highly polymerized melts. The rationale for this speculation is as follows. Most likely the principal depolymerized (NBO/T > 0) anionic unit in the highly polymerized Na_2O-Al_2O_3-SiO_2 melts has a $Si_2O_5^{2-}$ stoichiometry (Mysen, 1987; Mysen et al., 1982a; Furukawa et al., 1981). The stability of $Si_2O_5^{2-}$ units depends, however, on the type network-modifying cations present (Fig. 8). In melts on binary metal oxide–silica joins, the relative abundance of $Si_2O_5^{2-}$ units decreases rapidly with increasing Z/r^2 of the metal cation so that for MgO-SiO_2 melts, for example, $Si_2O_5^{2-}$ units can no longer be identified (Mysen, 1987; Mysen et al., 1982a). This reduction in abundance of $Si_2O_5^{2-}$ units caused by increasing Z/r^2 of the metal cation in binary metal oxide–silica melts is coupled with an increase in abundance of SiO_3^{2-} (NBO/Si = 2) and SiO_2 (NBO/Si = 0) units in order to maintain the overall bulk melt polymerization (Fig. 8; see also Mysen, 1987). Thus, in highly polymerized MgO-SiO_2 melts, the principal depolymerized structural unit has a SiO_3^{2-} stoichiometry (NBO/Si = 2). Principally similar conclusions were made by Liebau (1981) on the basis of size and charge distribution of the network-modifying cations in crystalline silicates. In analogy with crystal chemistry, it is suggested that melts on the join FeO-SiO_2 structurally resemble those on the join MgO-SiO_2. As can be seen from Figure 8, at the Z/r^2 corresponding to that of Fe^{2+}, the abundance of $Si_2O_5^{2-}$ units is negligible. Thus, it is possible that the activity coefficient of Fe^{2+} in melts may increase with decreasing NBO/T. Fe^{3+}, on the other hand, forms separate tetrahedral complexes (Virgo et al., 1983a; Virgo and Mysen, 1985), the geometry and composition of which appears insensitive to NBO/T and total Fe content. One might infer, therefore, that $\gamma_{Fe^{3+}}$ (activity coefficient of Fe^{3+}) is insensitive to NBO/T. Thus, there might be a minimum value of NBO/T of a melt below which the

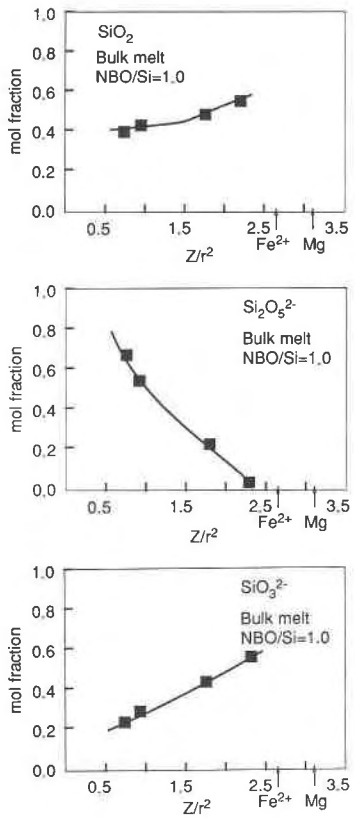

Fig. 8. Relationships between molar abundance of structural units in melts on metal oxide–silica joins and the Z/r^2 of the metal cation (data from Mysen et al., 1982a).

activity coefficient ratio, $\gamma_{Fe^{3+}}/\gamma_{Fe^{2+}}$, is so small that the concentration ratio, Fe^{3+}/Fe^{2+}, decreases with a further decrease in NBO/T. This model may rationalize the observed reversal in the relationship between NBO/T and $Fe^{3+}/\Sigma Fe$.

For melts with the same NBO/T (constant degree of polymerization), the $Fe^{3+}/\Sigma Fe$ is positively correlated with Al/(Al + Si) (Fig. 9) even when the Al/(Al + Si) variations do not involve changes in the degree of polymerization of the melts. Such relationships have also been found in the systems K_2O-Al_2O_3-SiO_2-Fe-O (Dickenson and Hess, 1981), CaO-Al_2O_3-SiO_2-Fe-O (Neumann et al., 1982), and MgO-Al_2O_3-SiO_2-Fe-O (Seifert et al., 1982b) with $K^+/Al^{3+} > 1.0$ and $M^{2+}/Al^{3+} > 0.5$ (M^{2+} = Ca and Mg). This dependence is more pronounced for reduced ($Fe^{3+}/\Sigma Fe < 0.6$) than for oxidized ($Fe^{3+}/\Sigma Fe > 0.6$) melts. The $Fe^{3+}/\Sigma Fe$ becomes more strongly dependent on Al/(Al + Si) the higher the temperature.

In order to express the interaction between the anionic aluminosilicate network and Fe^{3+} and Fe^{2+}, the influence of Al^{3+} on the melt structure must be considered. For aluminosilicate melts in the NBO/T range of the present study, the Al^{3+} will substitute preferentially for Si^{4+} in three-dimensional network units relative to other structural units (Mysen et al., 1981, 1985d; Domine and Pi-

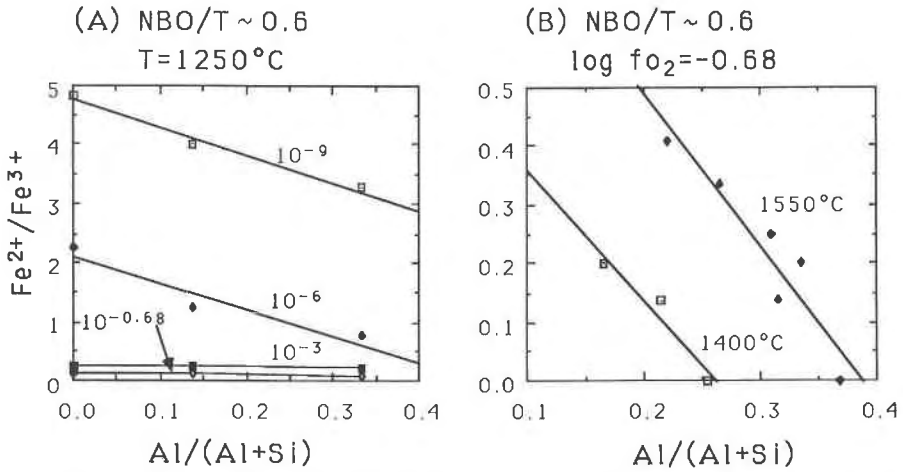

Fig. 9. Relationship between redox ratio of Fe and Al/(Al + Si) as a function of temperature and oxygen fugacity.

riou, 1986). This structural behavior is related to the observation that Al^{3+} will preferentially substitute for Si^{4+} in an interconnected network with the smallest available associated intertetrahedral angle (Brown et al., 1969). Among the structural units in silicate melts, three-dimensionally interconnected units have the smallest intertetrahedral angle (Furukawa et al., 1981). Consequently, along a composition join with constant NBO/T, the proportion of three-dimensional network units increases with increasing Al/(Al + Si) (Fig. 10).

In order to maintain the same bulk melt NBO/T, this increase in abundance of three-dimensional network units is compensated by enhanced relative abundance of depolymerized anionic units (their individual NBO/T values are greater than the NBO/T value of the bulk melt) (Fig. 10). The equilibria involving Al may be expressed with equations such as

$$SiO_2 + (NaAl)_2O_3^{2-} \rightleftharpoons SiO_3^{2-} + 2NaAlO_2, \quad (3)$$

and

$$Si_2O_5^{2-} + (NaAl)_2O_3^{2-} \rightleftharpoons 2SiO_3^{2-} + 2NaAlO_2. \quad (4)$$

Equations 3 and 4 may be combined with the trends in redox equilibria to yield expressions that interrelate the structural positions of Fe^{3+} and Fe^{2+} with the anionic structure of aluminosilicate melts,

$$7SiO_2 + Si_2O_5^{2-} + 2(NaAl)_2O_3^{2-} + 4FeO_2^- \rightleftharpoons 9SiO_3^{2-} + 4NaAlO_2 + 4Fe^{2+} + O_2, \quad (5)$$

with the equilibrium constant

$$K_5 = \frac{[SiO_3^{2-}]^9[NaAlO_2]^4}{[SiO_2]^7[Si_2O_5^{2-}][2(NaAl)_2O_3^{2-}]} \frac{[Fe^{2+}]^4}{[FeO_2^-]^4} f_{O_2}. \quad (6)$$

In Equation 5, the network-modifying Fe^{2+} most likely is associated with nonbridging oxygen in the $Si_2O_5^{2-}$ complex. The remaining nonbridging oxygen (in both $Si_2O_5^{2-}$ and $Si_2O_3^{2-}$ structural units) is bonded to network-modifying Na^+. With increasing Al/(Al + Si), both $[NaAlO_2]^4/[(NaAl)_2O_5^{2-}]^2$ and $[SiO_3^{2-}]^9/Si_2O_5^{2-}$ will increase. The proportional increase of SiO_3^{2-} equals that of SiO_2 to maintain constant bulk melt NBO/T. As a result, the $Fe^{3+}/\Sigma Fe$ will also increase.

The $Fe^{3+}/\Sigma Fe$ decreases with increasing temperature as is generally the case for silicate melts. For samples equilibrated with air, the slope of the log (Fe^{2+}/Fe^{3+}) vs. $1/T$ (K) curves is constant for a given composition (Fig. 11), but decreases slightly with increasing Al/(Al + Si) at similar NBO/T and with increasing NBO/T at the same Al/(Al + Si). At $f_{O_2} < 10^{-3}$ bar, the data indicate that at or above 1400 °C, the slope of the log (Fe^{2+}/Fe^{3+}) vs. $1/T$ curves steepens. This apparent change in slope coincides with the $Fe^{3+}/\Sigma Fe$ range where the hyperfine parameters for Fe^{3+} (Fig. 6) were interpreted to indicate the beginning of a coordination transformation of Fe^{3+}.

Redox equilibria and melt properties

Melt polymerization and redox equilibria

Melt polymerization, relative proportions of anionic units, and the distribution of Al^{3+} between these units depend on the $Fe^{3+}/\Sigma Fe$ of Fe-bearing silicate melts (see Eqs. 5 and 6). Furthermore, the transformation of Fe^{3+}

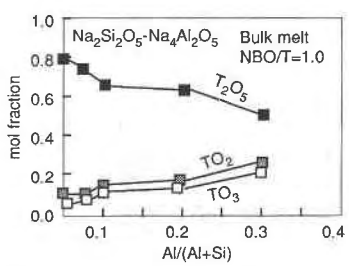

Fig. 10. Relationships between molar abundance of structural units denoted TO_2, T_2O_5, and TO_3 (T = Al + Si) as a function of Al/(Al + Si) along the sodium disilicate–sodium dialuminate join (data from Mysen et al., 1985d).

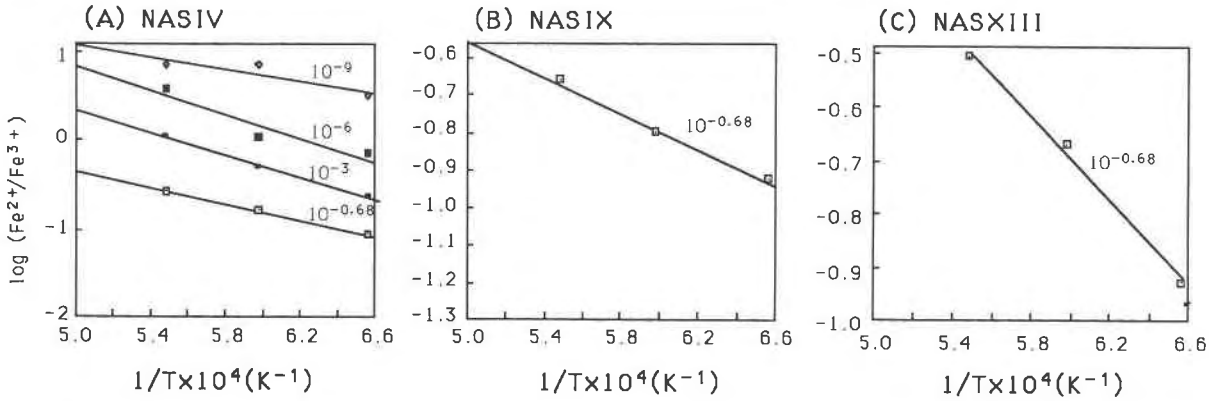

Fig. 11. Temperature dependence of redox ratio of Fe as a function of bulk melt composition (**A**: NASIVF5, **B**: NASIXF5, **C**: NASXIIIF5) at different oxygen fugacities (as indicated in figure).

from fourfold to sixfold coordination resulting from the reduction of some of the Fe^{3+} to Fe^{2+} will also affect the melt structure. Two examples to demonstrate the variation of NBO/T with $Fe^{3+}/\Sigma Fe$ are shown (Fig. 12), where the dashed line indicates that calculated changes of NBO/T with Fe^{3+} in fourfold coordination in the entire $Fe^{3+}/\Sigma Fe$ range from 1.0 to 0.0. The changes in NBO/T are calculated relative to the NBO/T values with $Fe^{3+}/\Sigma Fe = 1.0$ (all Fe^{3+} in tetrahedral coordination). The solid lines represent the NBO/T trajectory of NASIV melt [Al/(Al + Si) = 0.334, Fe-free NBO/T = 0.615, 5 wt% Fe_2O_3 (tetrahedral Fe^{3+}) NBO/T = 0.528] and NASIX [Al/(Al + Si) = 0.334, Fe-free NBO/T = 0.166, 5 wt% Fe_2O_3 (tetrahedral Fe^{3+}) NBO/T = 0.112] as a function of $Fe^{3+}/\Sigma Fe$ and $^{[6]}Fe^{3+}/\Sigma Fe^{3+}$ (calculated from $IS_{Fe^{3+}}$ vs. $Fe^{3+}/\Sigma Fe$, Fig. 6). Simple depolymerization by reduction of tetrahedrally coordinated Fe^{3+} to octahedrally coordinated Fe^{2+} is evident. The relative changes in NBO/T are greater the more

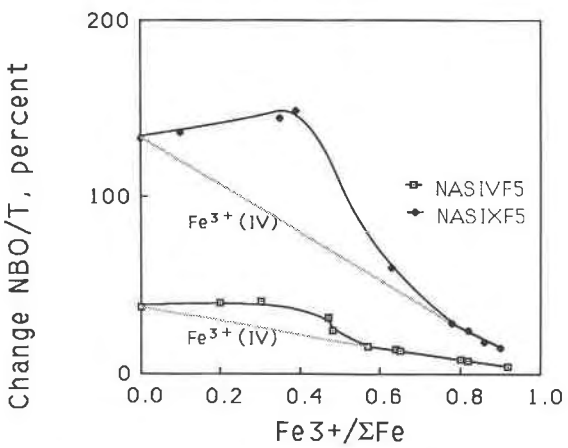

Fig. 12. Percent increase of NBO/T of melt compositions NASIVF5 and NASIXF5 relative to value calculated with $Fe^{3+}/\Sigma Fe$ equal to 1. Dotted lines represent hypothetical change in NBO/T of the two compositions with Fe^{3+} in tetrahedral coordination [Fe^{3+}(IV)] throughout the $Fe^{3+}/\Sigma Fe$ range. See text for detailed description of symbols.

polymerized the melt because the $d(NBO/T)/d(Fe^{3+}/\Sigma Fe)$ is approximately the same in both melt systems. The change in slope near $Fe^{3+}/\Sigma Fe = 0.6$ (Fig. 12) results from the $Fe^{3+}/\Sigma Fe$–controlled transformation of Fe^{3+} from fourfold to sixfold coordination (Fig. 6):

$$4SiO_2 + {}^{[4]}FeO_2^- \rightleftharpoons {}^{[6]}Fe^{3+} + 2Si_2O_5^{2-}. \quad (7)$$

Thus, in addition to depolymerization resulting from a reaction such as illustrated by Equation 2, further depolymerization results from the coordination of transformation (Eq. 7), and $d(NBO/T)/d(Fe^{3+}/\Sigma Fe)$ will increase at the onset of this transformation.

These two depolymerization effects are, however, countered by the fact that once Fe^{3+} is in octahedral coordination, its reduction to Fe^{2+} is associated with polymerization of the melt:

$$4^{[6]}Fe^{3+} + 2Si_2O_5^{2-} \rightleftharpoons 4^{[6]}Fe^{2+} + 2SiO_2 + O_2. \quad (8)$$

These three effects (Eqs. 2, 7, and 8) taken together result in the maxima of the depolymerization curves near $Fe^{3+}/\Sigma Fe = 0.3$–0.4 in Figure 12. The principal relations between $Fe^{3+}/\Sigma Fe$ and NBO/T (Fig. 12) can be used to calculate the degree of polymerization of silicate melts as a function of oxygen fugacity (Fig. 13) and temperature (Fig. 14). Decreasing f_{O_2} is systematically related to a decrease in $Fe^{3+}/\Sigma Fe$ (Fig. 15), and, therefore, degree of polymerization of the melt (Fig. 13). In Figure 13, the line marked "M" represents the NBO/T trajectory of composition NASIV (Table 1) with 5 wt% iron oxide added as Fe_2O_3 (NASIVF5). The dashed lines marked "IV" and "VI" represent hypothetical NBO/T trajectories under the assumption that Fe^{3+} was fourfold and sixfold coordinated, respectively, over the entire f_{O_2} range. The shaded regions are meant to highlight the NBO/T difference between "M" and the NBO/T value of the hypothetical "IV" curve in the $Fe^{3+}/\Sigma Fe$ range where Fe^{3+} undergoes its $Fe^{3+}/\Sigma Fe$–induced coordination transformation. The NBO/T values of the Fe-free NASIV and NASIVF5 with $Fe^{3+}/\Sigma Fe = 1.0$ for fourfold and sixfold coordination are also marked.

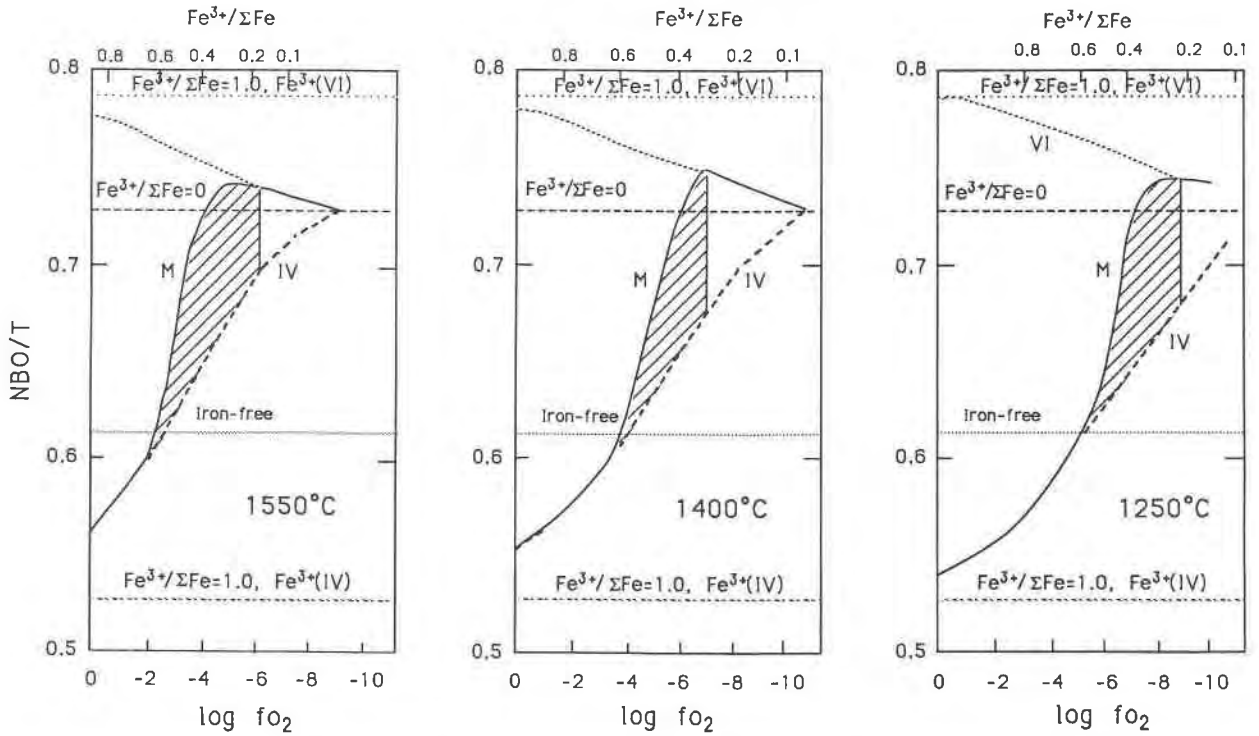

Fig. 13. Calculated change in NBO/T (as in Fig. 12) of sodium aluminosilicate melt NASIVF5 as a function of oxygen fugacity. See text for detailed description of symbols; (VI) = octahedral coordination; (IV) = tetrahedral coordination.

The topologies of the NBO/T vs. f_{O_2} curves at the three different temperature are qualitatively similar in that NBO/T increases as the f_{O_2} is lowered. Furthermore, there is an increase in $d(\text{NBO/T})/d(\text{Fe}^{3+}/\Sigma\text{Fe})$ as Fe^{3+} begins to undergo coordination transformation and subsequent change in sign when nearly all remaining Fe^{3+} has become a network modifier. Note, however, that the f_{O_2} corresponding to the onset and completion of Fe^{3+} coordination transformation decreases with increasing temperature. This difference stems from the temperature dependence of $Fe^{3+}/\Sigma Fe$ (Fig. 11).

The Al/(Al + Si) and NBO/T of NASIV composition correspond to those of high-alumina basalt (see Mysen, 1987, for compositional ranges and structure of natural magmatic liquids). The NASIV differs from natural magma in its lack of alkaline earths. Relationships quantitatively similar to those illustrated in Figure 13 exist, however, for the analogous compositions CASIV (CaO-Al_2O_3-SiO_2) and MASIV (MgO-Al_2O_3-SiO_2) (Mysen et al., 1985a). Thus, it is suggested that f_{O_2} variations of about two orders of magnitude may be sufficient to change the NBO/T of basaltic magma containing 5 wt% iron oxide by as much as 20%. In terms of typical magmatic liquids, this change is comparable to the difference in NBO/T between tholeiite and basaltic andesite liquids (see also Mysen, 1987). With higher iron oxide contents, the effect of f_{O_2} on the degree of polymerization of basaltic magma becomes bigger.

The oxygen fugacity is, therefore, not only important in governing redox equilibria in natural basaltic magma, but is also an important variable in controlling the overall degree of polymerization and, therefore, all melt properties that are related to this variable (e.g., liquidus phase relations, viscous behavior, crystal-liquid trace-element partitioning, and mixing properties).

In Figure 14, the NBO/T trajectories of NASIVF5 melt have been calculated as a function of temperature at three different oxygen fugacities. The symbols are the same as in Figure 13. The temperature range considered corresponds to that of most magmatic liquids at or above their liquidii at 1 bar. If the melt is equilibrated with air, reduction of $^{[4]}Fe^{3+}$ to $^{[6]}Fe^{2+}$ is the only relevant process and a 10% increase in NBO/T is realized by reducing the Fe from 100% Fe^{3+} to 100% Fe^{2+}. At $f_{O_2} = 10^{-3}$ bar, however, the temperature has a much greater effect because, at temperatures slightly above 1400 °C, the $Fe^{3+}/\Sigma Fe$ is sufficiently low (see Figs. 6 and 11) that Fe^{3+} begins to transform from fourfold to sixfold coordination. As a result, a nearly 40% increase in NBO/T is realized in the 1200–1700 °C temperature range. At $f_{O_2} = 10^{-6}$ bar, the temperature effect is somewhat less pronounced simply because even at 1200 °C, the $Fe^{3+}/\Sigma Fe$ is significantly lower than at 10^{-3} bar (0.64 compared with 0.85). Thus, the amount of $Fe^{3+}/\Sigma Fe$ reduction and, therefore, the temperature increase necessary to convert all Fe^{3+} from a network-former to a network-modifier are smaller at f_{O_2}

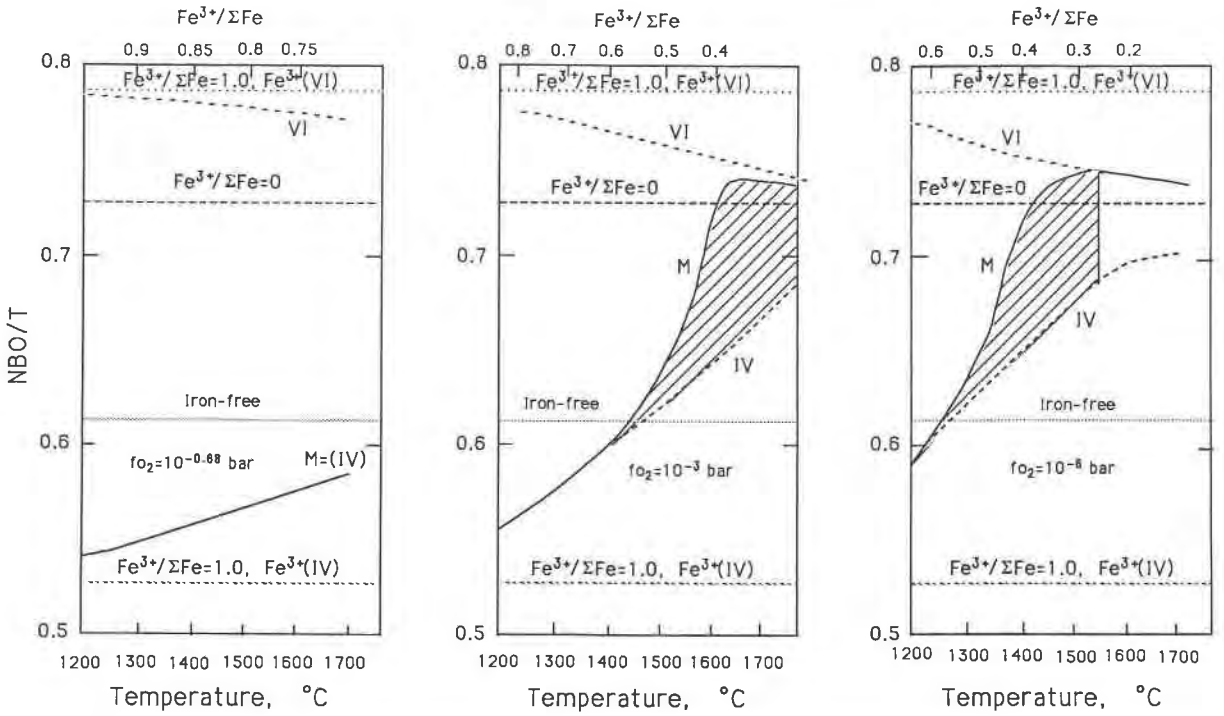

Fig. 14. Calculated change in NBO/T (as in Fig. 12) of sodium aluminosilicate melt NASIVF5 as a function of temperature. See text for detailed description of symbols; (VI) = octahedral coordination; (IV) = tetrahedral coordination.

$= 10^{-6}$ bar than at $f_{O_2} = 10^{-3}$ bar. A consequence of the results in Figure 14 is that as a magma cools (e.g., during ascent through the mantle and crust) along its liquidus, it becomes significantly more oxidized and, therefore, more polymerized. If, in addition, the effect of pressure on $Fe^{3+}/\Sigma Fe$ at constant f_{O_2} is taken into consideration (see, for example, Mo et al., 1982, and Mysen and Virgo, 1978, 1985, for relationships between $Fe^{3+}/\Sigma Fe$ and pressure), the ascent itself (decompression) will also enhance oxidation of Fe, thus further polymerizing the liquid.

Viscosity and redox equilibria

Most properties of silicate melts and melt-mineral systems depend on the degree of polymerization of the melt. An example is melt viscosity. Klein et al. (1983) and more recently Dingwell and Virgo (1987) have demonstrated that the $Fe^{3+}/\Sigma Fe$ ratio of Fe-bearing silicate glasses and melts affects the melt viscosity. In particular, Dingwell and Virgo (1987), in a study where results of Mössbauer spectroscopy of quenched Na_2O-SiO_2-Fe-O glasses were combined with viscometry in the superliquidus region, demonstrated that the viscous behavior of those liquids was closely related to the NBO/T of the melt controlled by the $Fe^{3+}/\Sigma Fe$. They showed, for example (their Figs. 2 and 3), that the melt viscosity decreased systematically as a function of decreasing $Fe^{3+}/\Sigma Fe$ until $Fe^{3+}/\Sigma Fe$ reached ~0.4–0.3. With a further decrease of $Fe^{3+}/\Sigma Fe$, no further decrease in melt viscosity

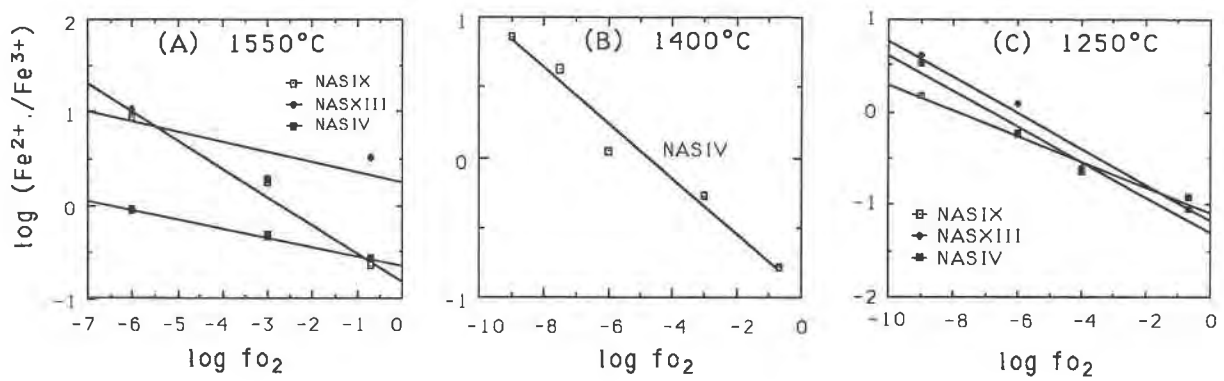

Fig. 15. Relations between oxygen fugacity and redox ratio of Fe at different temperatures as a function of NBO/T and Al/(Al + Si) of the melt.

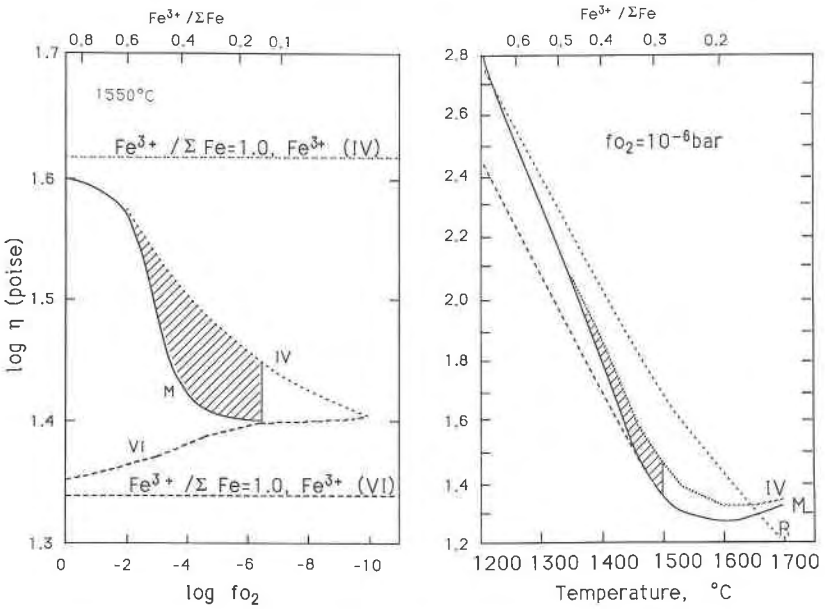

Fig. 16. Calculated changes in viscosity of NASIVF5 melt as a function of oxygen fugacity and temperature. See text for detailed description of symbols; (VI) = octahedral coordination; (IV) = tetrahedral coordination.

was observed. This viscous behavior was correlated with melt depolymerization as a function of $Fe^{3+}/\Sigma Fe$ as $^{[4]}Fe^{3+}/^{[6]}Fe^{2+}$ decreased. The absence of such a relationship for $Fe^{3+}/\Sigma Fe < 0.4$ was ascribed to the $Fe^{3+}/\Sigma Fe$–controlled coordination transformation of Fe^{3+}. Those viscosity data could not be rationalized if Fe^{3+} remained in tetrahedral coordination over the entire $Fe^{3+}/\Sigma Fe$ range, or if a significant portion of Fe^{2+} was in tetrahedral coordination. Recently, Dingwell et al. (1988) made similar conclusions on the basis of partial molar volumes of Fe^{2+} and Fe^{3+} in melts in the same system.

Thus, one may use the redox equilibria in Fe-bearing Na_2O-Al_2O_3-SiO_2 melts to illustrate, at least qualitatively, how oxygen fugacity and temperature may affect viscous behavior differently than in Fe-free melts (Fig. 16). The symbols "M," "IV," "VI," "$Fe^{3+}/\Sigma Fe = 1.0$, Fe^{3+}(IV)" (i.e., $^{[4]}Fe^{3+}$) and "$Fe^{3+}/\Sigma Fe = 1.0$, Fe^{3+}(VI)" (i.e., $^{[6]}Fe^{3+}$) have the same meaning as in Figures 13 and 14. The viscosities were calculated with the scheme proposed by Bottinga and Weill (1972). In the calculations of melt viscosity, the variations in NBO/T, governed by $Fe^{3+}/\Sigma Fe$, were recalculated as an equivalent melt composition in the system Na_2O-Al_2O_3-SiO_2. Thus, the influence of Fe itself on the viscosity was neglected. Addition of Fe would tend to lower the viscosity compared with the Fe-free end member (Mysen et al., 1985c; Dingwell and Virgo, 1987). In view of the relatively low Fe content (5 wt%), this simplification most likely has a relatively small effect.

At 1550 °C, the $Fe^{3+}/\Sigma Fe$ ranges from 0.94 to nearly 0 over the f_{O_2} range used for the calculations in Figure 16. In this f_{O_2} range (10^0 to 10^{-10} bar), the viscosity at 1550 °C will decrease by at least 37%. Because of the rapid depolymerization as Fe^{3+} undergoes coordination transformation (ruled area), about 80% of this decrease takes place over slightly more than a one order of magnitude decrease in f_{O_2}. At 1550 °C, this f_{O_2} range is from 1.5 orders of magnitude above the f_{O_2} of the nickel–nickel oxide (NNO) buffer down to approximately the value defined by the NNO oxygen buffer. Because the reduction of $^{[6]}Fe^{3+}$ to Fe^{2+} acts as a mechanism of melt polymerization, at lower oxygen fugacity there is very little effect on f_{O_2} on the melt viscosity.

In terms of the overall topology, these calculated variations resemble those measured by Dingwell and Virgo (1987) in the simpler system Na_2O-SiO_2-Fe-O (see their Fig. 7). Because the temperature affects $Fe^{3+}/\Sigma Fe$ and, therefore NBO/T, the viscosity vs. temperature relations (Fig. 16) are different from those of Fe-free melts. The curve marked "R" represents the viscosity vs. temperature trajectory of a melt composition whose NBO/T is identical to that of NASIVF5 at 1250 °C and does not change with temperature. Its trajectory follows that of a common Arrhenius relationship:

$$\ln \eta = \ln \eta_0 + (E_\eta/RT), \tag{9}$$

where η is viscosity, E_η is activation energy of viscous flow, T is absolute temperature, R is the gas constant, and η_0 is a constant.

For NASIVF5, on the other hand, the NBO/T increases with increasing temperature (Fig. 14). Consequently, the activation energy of viscous flow, E_η, decreases with increasing temperature, and the viscosity decreases more rapidly with increasing temperature than the trend described by the temperature effect alone.

The viscosity trajectory gradually changes with increasing temperature from that defined by "R" and follows

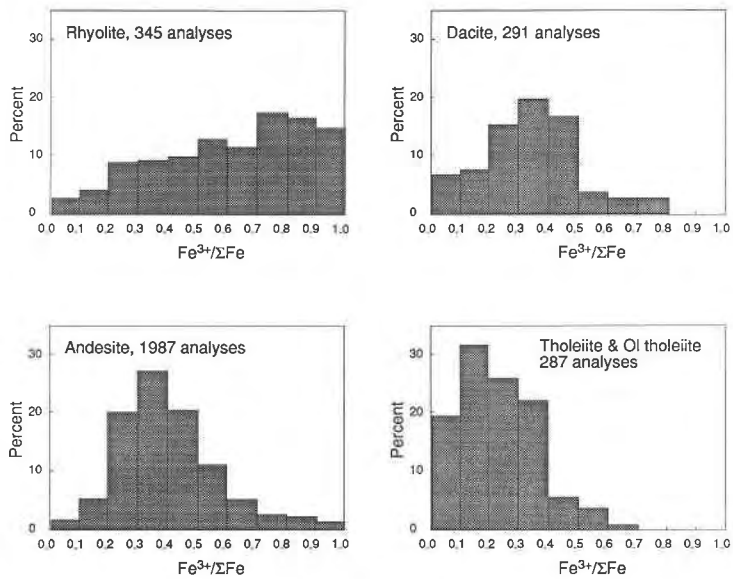

Fig. 17. Distribution of $Fe^{3+}/\Sigma Fe$ from extrusive igneous rocks as named (database RKNFSYS from Chayes, 1975a, 1975b, unpub. document, 1985).

that defined by fourfold-coordinated Fe^{3+} (but with $Fe^{3+}/\Sigma Fe$ decreasing) until the Fe^{3+} coordination change begins (ruled area). In this $Fe^{3+}/\Sigma Fe$ range, the viscosity trajectory shifts from that defined by "IV" to that defined by "VI." Finally, the trajectory coincides with that defined by a melt where Fe^{3+} is in octahedral coordination. A maximum viscosity difference between "R" and "M" of slightly more than 50% exists at temperatures near 1500 °C.

Redox equilibria in natural magmatic systems

The rock file RKNFSYS contains slightly above 16000 analyses of Cenozoic volcanic rocks (Chayes, 1975a, 1975b; Chayes, unpub. document, 1985). This rock file provides the opportunity to extract bulk compositional information based on (1) rock names used in the original sources, (2) geographic distributions, (3) age, or (4) chemical discriminants. For the following application, analyses from selected groups of rocks were extracted, and their reported chemical compositions were treated as if these represented the compositions of their respective liquids. It is recognized that this approach is a significant simplification as subliquidus and subsolidus processes easily could have altered the redox ratios of Fe. The data are used, however, to point out certain systematics that seem to exist between major groups of igneous rocks. No attempt has been made to refine or redefine the names used in the original sources of the RKNFSYS. Furthermore, as it is considered unlikely that an unaltered extrusive igneous rock will contain more than 2 wt% H_2O, analyses with more than this amount of water have not been used. Finally, this collection of analyses is by no means exhaustive, but it is hoped to be representative.

The $Fe^{3+}/\Sigma Fe$ ratios of extrusive igneous rocks range from near 0 to 1.0 (Fig. 17). From the data compilation in Figure 17, it is notable, however, that the distribution in $Fe^{3+}/\Sigma Fe$ appears greater for the most felsic rock groups and in particular for rhyolite and, in general, the average $Fe^{3+}/\Sigma Fe$ decreases for the more mafic melt compositions (Table 3).

TABLE 3. Percentage of analyses (rock analyses from Chayes, 1975a, 1975b, unpub. document, 1985) where $Fe^{3+}/\Sigma Fe$ falls within the brackets indicated

	Rhyolite	Dacite	Andesite	Tholeiite and olivine tholeiite	Alkali basalt	Nephelinite
No. of analyses	367	338	2068	1010	279	116
$Fe^{3+}/\Sigma Fe$*	0.63 ± 0.25	0.48 ± 0.20	0.40 ± 0.07	0.29 ± 0.13	0.38 ± 0.19	0.43 ± 0.16
<0.3**	13.9	23.3	28.9	58.3	36.6	23.3
0.3–0.6**	17.2	43.1	49.7	34.7	40.1	43.1
>0.6**	68.9	33.6	21.5	7.0	23.3	33.6

* Average values for rock group.

** With $Fe^{3+}/\Sigma Fe < 0.3$, all Fe^{3+} is considered to be in octahedral coordination, with $Fe^{3+}/\Sigma Fe > 0.6$, all Fe^{3+} is considered to be in tetrahedral coordination, and with $Fe^{3+}/\Sigma Fe = 0.3$–0.6, tetrahedral and octahedral Fe^{3+} coexist in the melt.

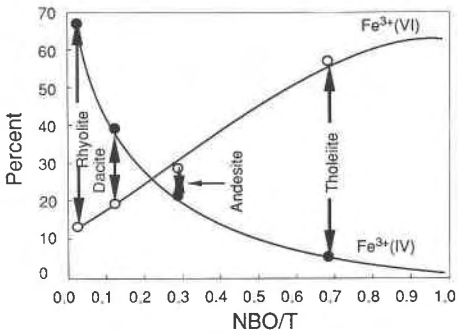

Fig. 18. Relative abundance of tetrahedrally coordinated Fe^{3+} [Fe^{3+}(IV)] and octahedrally coordinated Fe^{3+} [Fe^{3+}(VI)] in major groups of extrusive igneous rocks shown as a function of degree of polymerization of the melt. Values are calculated based on the average $Fe^{3+}/\Sigma Fe$ (from Table 3) for the rock groups indicated (database RKNFSYS from Chayes, 1975a, 1975b, unpub. document, 1985).

Under the assumption that the analyzed $Fe^{3+}/\Sigma Fe$ represents the $Fe^{3+}/\Sigma Fe$ of these materials prior to crystallization, the proportion of Fe^{3+} in octahedral and tetrahedral coordination can be estimated from the $Fe^{3+}/\Sigma Fe$ dependence of Fe^{3+} coordination in silicate melts. From the chosen selection of analyses in rock file RKNFSYS, the percentage of analyses with $Fe^{3+}/\Sigma Fe > 0.6$ (all Fe^{3+} in tetrahedral coordination) and $Fe^{3+}/\Sigma Fe < 0.3$ (all Fe^{3+} in octahedral coordination) have been plotted against the bulk melt NBO/T (Fig. 18). It is evident from the results in Figure 18 that the more felsic the rock (and, therefore, the more polymerized the melt), the ore prevalent is tetrahedrally coordinated Fe^{3+}. For rhyolite melts, for example, Fe^{3+} is commonly in tetrahedral coordination, whereas for tholeiitic and more mafic melts, octahedrally coordinated Fe^{3+} is common, and Fe^{3+} in tetrahedral coordination is an uncommon situation. A consequence of this observation is that during fractional crystallization of basaltic liquid toward andesite or rhyolite, the residual liquids become more polymerized not only because of increasing silica (and, perhaps, alumina) content. The process also appears to be associated with increasing $Fe^{3+}/\Sigma Fe$. This increase is so large that a significant fraction of the Fe^{3+} undergoes a coordination change and becomes a network former, thus further polymerizing the liquids.

Sack et al. (1980) pioneered the use of laboratory-calibrated $Fe^{3+}/\Sigma Fe$ as a function of temperature and oxygen fugacity as a calibrant for oxygen fugacity during formation of igneous rocks. These investigators employed an expression of the form

$$\ln(X_{Fe_2O_3}/X_{FeO}) = a + \frac{b}{T} + c \ln f_{O_2} + \sum_{i=1}^{i} d_i X_i, \quad (10)$$

where a, b, c, and d_i are regression coefficients, T is absolute temperature, $\ln f_{O_2}$ is the natural logarithm of the oxygen fugacity, and X_i is the concentration of the ith oxide component. By fitting 57 analyses from experimentally equilibrated liquids to this expression, Sack et al. (1980) found positive correlation of $\ln(X_{Fe_2O_3}/X_{FeO})$ with X_{Na_2O}, X_{K_2O}, and X_{CaO}, whereas X_{MgO}, $X_{Al_2O_3}$, and X_{FeO} were negatively correlated. In a subsequent refinement of this treatment, Kilinc et al. (1983) concluded that the Fe^{3+}/Fe^{2+} ratio depended only on X_{CaO}, X_{Na_2O}, X_{K_2O}, X_{FeO} (all positively correlated), and $X_{Al_2O_3}$ (negatively correlated). Kilinc et al. (1983) concluded that $X_{Fe_2O_3}/X_{FeO}$ was independent of X_{MgO} content of the liquid. X_{MgO} was not identified as a variable in the experimental results reported by Thornber et al. (1980).

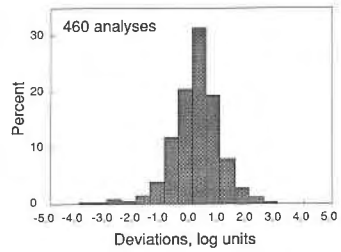

Fig. 19. Distribution of deviation of calculated oxygen fugacities (from Eq. 11) relative to experimental values (database as in Table 4).

Mysen (1987) suggested that the approach advanced by Sack et al. (1980) could be refined and linear regression could be applied to a rock composition after it has been recast to the relevant structural components. The procedure used to calculate the relevant structural components was described by Mysen (1987) and will not be repeated here. The structural components are those found to govern $Fe^{3+}/\Sigma Fe$ in binary and ternary systems. An expression of the form

$$\ln(X_{Fe^{2+}}/X_{Fe^{3+}}) = a + \frac{10^4 b}{T} + c \ln f_{O_2} + d\left(\frac{X_{Al}}{X_{Al} + X_{Si}}\right) + e\left(\frac{X_{Fe^{3+}}}{X_{Fe^{3+}} + X_{Si}}\right) + \sum_{j=1}^{j} f_j \left(\frac{NBO}{T}\right)_j, \quad (11)$$

TABLE 4. Regression coefficients for Equation 11

	Coefficient	Standard error
a (constant)	15.435	0.786
b (1/T)	−2.848	0.138
c (ln f_{O_2})	−0.3484	0.120
d [$Al^{3+}/(Al^{3+} + Si)$]	−1.309	0.469
e [$Fe^{3+}/(Fe^{3+} + Si)$]	−2.121	1.055
f_j (NBO/T)^{Mg}	0.6662	0.0966
f_j (NBO/T)^{Ca}	−0.5255	0.1084
f_j (NBO/T)^{Na}	−1.125	0.179
f_j (NBO/T)$^{Fe^{2+}}$	−3.215	0.538

Note: Numbers of analyses in regression = 460. Experimental data from Kennedy (1948), Fudali (1965), Sack et al. (1980), Thornber et al. (1980), Kilinc et al. (1983), Seifert et al. (1979), Virgo et al. (1981), Mysen and Virgo (1983), Virgo and Mysen (1985), Mysen et al. (1980, 1984, 1985a, 1985b, 1985c, 1985d).

can be describe the relationship between Fe^{2+}/Fe^{3+}, temperature, oxygen fugacity, and melt structure. The f_j and $(NBO/T)_j$ are the regression coefficients and NBO/T values of the structural units associated with individual network-modifying cations (j), respectively. The coefficients a, b, c, d, and e together with f_j are obtained with stepwise linear regression. Equation 11 takes into account each of the variables identified as affecting $Fe^{3+}/\Sigma Fe$.

The resulting coefficients are shown in Table 4. It is evident from this exercise that among the network-modifying cations, the $\ln(X_{Fe^{2+}}/X_{Fe^{3+}})$ is negatively correlated with the proportion of nonbridging oxygen associated with Ca^{2+}, Na^{+}, and Fe^{2+} (Table 4). The analysis shows that Fe^{2+}/Fe^{3+} increases with increasing NBO/T associated with Mg^{2+}. It is not clear why Mg^{2+} is an exception among the network-modifying cations in this respect. There is also a rapid decrease in $\ln(X_{Fe^{2+}}/X_{Fe^{3+}})$ with increasing $X_{Fe^{3+}}/(X_{Fe^{3+}} + X_{Si^{4+}})$ and with increasing $X_{Al}/(X_{Al} + X_{Si})$.

The coefficients in Table 4 may be inserted in Equation 11 to be used as an oxygen-fugacity barometer. The calculated f_{O_2} values for the samples in the dataset are compared with the measured values in Figure 19. Between 85 and 90% of the calculated values are within ± 1.0 log unit of the measured value, and 54% of the analyses are within ± 0.5 log unit of oxygen fugacity. About 95% fall within ± 1.5 log unit. It is suggested that this model relating redox ratios of Fe to temperature and melt structure is an adequate description and that Equation 11, with the coefficients in Table 4, can be used with confidence to calculate oxygen-fugacity conditions of natural magmatic liquids at 1 bar.

Acknowledgments

Critical reviews by R. W. Luth, C. T. Prewitt, and two anonymous reviewers are appreciated.

References cited

Amthauer, G., Annersten, H., and Hafner, S.S. (1977) The Mössbauer spectrum of ^{57}Fe in titanium-bearing andradites. Physics and Chemistry of Minerals, 1, 399–413.

Amthauer, G., Langer, K., and Schliestedt, M. (1980) Thermally activated electron delocalization in deerite. Physics and Chemistry of Minerals, 6, 19–30.

Annersten, H. (1976) New Mössbauer data on iron in potash feldspar. Neues Jahrbuch für Mineralogie, 8, 337–343.

Annersten, H., and Hafner, S.S. (1973) Vacancy distribution in synthetic spinels of the series Fe_3O_4-γFe_2O_3. Zeitschrift für Kristallographie, 137, 321–340.

Annersten, H., and Olesch, M. (1978) Distribution of ferrous and ferric iron in clintonite and the Mössbauer characteristics of ferric iron in tetrahedral coordination. Canadian Mineralogist, 16, 199–204.

Annersten, H., Olesch, M., and Seifert, F.A. (1978) Ferric iron in orthopyroxene: A Mössbauer spectroscopy study. Lithos, 11, 301–310.

Bockris, J.O'M., and Kojonen, F. (1960) The compressibility of certain molten alkali silicates and borates. Journal of the American Ceramic Society, 82, 4493–4497.

Bockris, J.O'M., and Reddy, A.K.N. (1970) Modern electrochemistry, vol. 1, 622 p. Plenum Press, New York.

Bottinga, Y., and Weill, D.F. (1972) The viscosity of magmatic silicate liquids: A model for calculation. American Journal of Science, 272, 438–475.

Bottinga, Y., Weill, D.F., and Richet, P. (1982) Density calculations for silicate liquids. I. Revised method for aluminosilicate compositions. Geochima et Cosmochimica Acta, 46, 909–919.

Bottinga, Y., Richet, P., and Weill, D.F. (1983) Calculation of the density and thermal expansion coefficient of silicate liquids. Bulletin Minéralogique, 106, 129–138.

Bowen, N.L., Schairer, J.F., and Willems, H.W.V. (1930) The ternary system Na_2SiO_3-Fe_2O_3-SiO_2. American Journal of Science, 20, 405–455.

Brown, G.E., Gibbs, G.V., and Ribbe, P.H. (1969) The nature and variation in length of Si–O and Al–O bonds in framework silicates. American Mineralogist, 54, 1044–1061.

Burnham, C.W. (1981) The nature of multicomponent aluminosilicate melts. Physics and Chemistry of the Earth, 13 and 14, 197–227.

Calas, G., and Petiau, J. (1983a) Coordination of iron in oxide glasses through high-resolution K-edge spectra: Information from the pre-edge. Solid State Communications, 48, 625–629.

——— (1983b) Structure of oxide glasses: Spectroscopic studies of local order and crystallochemistry: Geochemical implications. Bulletin Minéralogique, 106, 33–53.

Chayes, F. (1975a) A world data base for igneous petrology. Carnegie Institution of Washington Year Book 74, 549–550.

——— (1975b) Average composition of the commoner Cenozoic volcanic rocks. Carnegie Institution of Washington Year Book 74, 547–549.

Chou, I.-M. (1978) Calibration of oxygen buffers at high P and T using the hydrogen fugacity sensor. American Mineralogist, 63, 690–703.

Coey, J.M.D., Moukarika, A., and McDonagh, C.M. (1982) Electron hopping in cronstedtite. Solid State Communications, 41, 797–800.

Cooney, T., Sharma, S.K., and Urmos, J.P. (1987) Structure of glasses along the forsterite-fayalite and tephroite-fayalite join. EOS, p. 436.

Deines, P., Nafziger, R.H., Ulmer, G.C., and Woermann, E. (1974) Temperature–oxygen fugacity tables for selected gas mixtures in the system C-H-O at one atmosphere total pressure. Bulletin of the Earth and Mineral Sciences Experiment Station, no. 88. Pennsylvania State University, University Park, Pennsylvania.

Dickenson, M.P., and Hess, P.C. (1981) Redox equilibria and the structural role of iron in aluminosilicate melts. Contributions to Mineralogy and Petrology, 78, 352–358.

——— (1986) The structural role and homogeneous redox equilibria of iron in peraluminous, metaluminous, and peralkaline silicate melts. Contributions to Mineralogy and Petrology, 92, 207–217.

Dingwell, D.B., and Virgo, D. (1987) The effect of oxidation state on the viscosity of melts in the system Na_2O-FeO-Fe_2O_3-SiO_2. Geochimica et Cosmochimica Acta, 51, 195–205.

Dingwell, D.B., Brearley, M., and Dickinson, J.E. (1988) Melt densities in the Na_2O-FeO-Fe_2O_3-SiO_2 system and partial molar volume of tetrahedrally coordinated ferric iron in silicate melts. Geochimica et Cosmochimica Acta, 52, 2467–2476.

Domine, F., and Piriou, B. (1986) Raman spectroscopic study of the SiO_2-Al_2O_3-K_2O vitreous system: Distribution of silicon and second neighbors. American Mineralogist, 71, 38–50.

Douglas, E.W., North, P., and Paul, A. (1965) Oxygen ion activity and its influence on the redox equilibrium in glasses. Physics and Chemistry of Glasses, 6, 215–223.

Dyar, M.D., and Birnie, D.P. (1984) Quench media effects on iron partitioning in a lunar glass. Journal of Non-Crystalline Solids, 67, 397–412.

Dyar, M.D., Naney, M.T., and Swanson, S.E. (1987) Effect of quench methods on Fe^{3+}/Fe^{2+} ratios: A Mössbauer and wet-chemical study. American Mineralogist, 72, 792–800.

Evans, B.J., and Amthauer, G. (1980) The electronic structure of ilvaite and the pressure and temperature dependence of its ^{57}Fe Mössbauer spectrum. Journal of the Physics and Chemistry of Solids, 41, 985–1007.

Fox, K.E., Furukawa, T., and White, W.B. (1982) Transition metal ions in silicate melts. Part 2. Iron in sodium silicate glasses. Physics and Chemistry of Glasses, 23, 167–178.

Fraser, D.G., Rammensee, W., and Jones, R.H. (1983) The mixing properties of melts in the system $NaAlSi_2O_6$-$KAlSi_2O_6$ determined by Knudsen cell mass spectrometry. Bulletin Minéralogique, 106, 111–117.

Fudali, F. (1965) Oxygen fugacity of basaltic and andesitic magmas. Geochimica et Cosmochimica Acta, 29, 1063–1075.

Furukawa, T., Fox, K.E., and White, W.B. (1981) Raman spectroscopic investigation of the structure of silicate glasses. III. Raman intensities and the structural units in sodium silicate glasses. Journal of Chemical Physics, 75, 3226–3237.

Glasser, F.P., Woodhams, F.W.D., Meads, R.E., and Parker, W.G. (1972) A Mössbauer and ESR study of $CaO{\cdot}6Al_2O_3$-$CaO{\cdot}6Fe_2O_3$ solid solutions. Journal of Solid State Chemistry, 5, 255–261.

Goldman, D.S., and Berg, J.I. (1980) Spectral study of ferrous iron in Ca-Al borosilicate glass at room and melt temperatures. Journal of Non-Crystalline Solids, 38 and 39, 183–188.

Grandjean, F., and Gerard, A. (1978) Observation by Mössbauer spectroscopy of electron hoppings in the spinel series $Zn_{1-x}Ge_xFe_2O_4$. Solid State Communications, 25, 679–683.

Hafner, S.S., and Huckenholz, H.G. (1971) Mössbauer spectrum of synthetic ferridiopside. Nature, 233, 255–261.

Haggstrom, L., Annersten, H., Ericsson, T., Wappling, R., Karner, W., and Bjarman, S. (1978) Magnetic dipolar and electric quadrupolar effects on the Mössbauer spectra of magnetite above the Verwey transition. Hyperfine Interactions, 5, 201–214.

Hofmann, A.W., and Magaritz, M. (1977) Diffusion of Ca, Sr, Ba, and Co in a basalt melt: Implications for the geochemistry of the mantle. Journal of Geophysical Research, 83, 5432–5441.

Holmquist, S. (1966) Ionic formulation of redox equilibria in glass melts. Journal of the American Ceramic Society, 49, 228–229.

Huggins, F.E., Virgo, D., and Huckenholz, H.G. (1977) Titanium-containing silicate garnets. II. The crystal chemistry of melanites and schorlomites. American Mineralogist, 62, 646–665.

Kennedy, G.C. (1948) Equilibrium between volatiles and iron oxides in rocks. American Journal of Science, 246, 529–549.

Kilinc, A., Carmichael, I.S.E., Rivers, M.L., and Sack, R.O. (1983) The ferric-ferrous ratio of natural silicate liquids equilibrated in air. Contributions to Mineralogy and Petrology, 83, 136–141.

Klein, L.C., Fasano, B., and Wu, J.M. (1983) Viscous flow behavior of four iron-containing silicates with alumina, effects of composition and oxidation conditions. Journal of Geophysical Research, 88, 880–886.

Kushiro, I. (1975) On the nature of silicate melt and its significance in magma genesis: Regularities in the shift of liquidus boundaries involving olivine, pyroxene, and silica minerals. American Journal of Science, 275, 411–431.

Larson, H., and Chipman, J. (1953) Oxygen activity in iron oxide slags. American Institute of Mining Engineers Transactions, 196, 1089–1096.

Liebau, F. (1981) The influence of cation properties on the conformation of silicate and phosphate anions. In M. O'Keeffe and A. Navrotsky, Eds., Structure and bonding in crystals, vol. 1, p. 197–232. Academic Press, New York.

Mao, H.-K., Virgo, D., and Bell, P.M. (1973) Analytical study of the orange soil returned by the Apollo 17 astronauts. Carnegie Institution of Washington Year Book 72, 631–638.

Matson, D.W., Sharma, S.K., and Philpotts, J.A. (1983) The structure of high-silica alkali-silicate glasses—A Raman spectroscopic investigation. Journal of Non-Crystalline Solids, 58, 323–352.

Mo, X.X., Carmichael, I.S.E., Rivers, M., and Stebbins, J. (1982) The partial molar volume of Fe_2O_3 in multicomponent silicate liquids and the pressure dependence of oxygen fugacity in magmas. Mineralogical Magazine, 45, 237–245.

Muan, A., and Osborn, E.F. (1965) Phase equilibria among oxides in steelmaking. 236 p. Addison-Wesley, Inc., Reading, Massachusetts.

Mysen, B.O. (1987) Magmatic silicate melts: Relations between bulk composition, structure, and properties. In B. O. Mysen, Ed., Magmatic processes: Physicochemical principles, Geochemical Society Special Publication 1, p. 375–399. Geochemical Society, University Park, Pennsylvania.

Mysen, B.O., and Virgo, D. (1978) Influence of pressure, temperature, and bulk composition on melt structures in the system $NaAlSi_2O_6$-$NaFe^{3+}Si_2O_6$. American Journal of Science, 278, 1307–1322.

——— (1980) Trace element partitioning and melt structure: An experimental study at 1 atm pressure. Geochimica et Cosmochimica Acta, 44, 1917–1930.

——— (1983) Effect of pressure on the structure of iron-bearing silicate melts. Carnegie Institution of Washington Year Book 82, 321–325.

——— (1985) Iron-bearing silicate melts: Relations between pressure and redox equilibria. Physics and Chemistry of Minerals, 12, 191–200.

Mysen, B.O., Seifert, F.A., and Virgo, D. (1980) Structure and redox equilibria of iron-bearing silicate melts. American Mineralogist, 65, 867–884.

Mysen, B.O., Virgo, D., and Kushiro, I. (1981) The structural role of aluminum in silicate melts—A Raman spectroscopic study at 1 atmosphere. American Mineralogist, 66, 678–701.

Mysen, B.O., Virgo, D., and Seifert, F.A. (1982a) The structure of silicate melts: Implications for chemical and physical properties of natural magma. Reviews of Geophysics, 20, 353–383.

Mysen, B.O., Finger, L.W., Virgo, D., and Seifert, F.A. (1982b) Curve-fitting of Raman spectra of silicate glasses. American Mineralogist, 67, 686–695.

Mysen, B.O., Virgo, D., and Seifert, F.A. (1984) Redox equilibria of iron in alkaline earth silicate melts: Relations between melt structure, oxygen fugacity, temperature, and properties of iron-bearing silicate liquids. American Mineralogist, 69, 834–848.

Mysen, B.O., Virgo, D., Neumann, E.-R., and Seifert, F.A. (1985a) Redox equilibria and the structural states of ferric and ferrous iron in melts in the system CaO-MgO-Al_2O_3-SiO_2: Relations between redox equilibria, melt structure, and phase equilibria. American Mineralogist, 70, 317–322.

Mysen, B.O., Carmichael, I.S.E., and Virgo, D. (1985b) A comparison of iron redox ratios in silicate glasses determined by wet-chemical and ^{57}Fe Mössbauer resonant absorption methods. Contributions to Mineralogy and Petrology, 90, 101–106.

Mysen, B.O., Virgo, D., Scarfe, C.M., and Cronin, D.J. (1985c) Viscosity and structure of iron- and aluminum-bearing calcium silicate melts. American Mineralogist, 70, 487–498.

Mysen, B.O., Virgo, D., and Seifert, F.A. (1985d) Relations between properties and structure of aluminosilicate melts. American Mineralogist, 70, 834–847.

Navrotsky, A., Peraudeau, P., McMillan, P., and Coutoures, J.-P. (1982) A thermochemical study of glasses and crystals along the joins silica–calcium aluminate and silica–sodium aluminate. Geochimica et Cosmochimica Acta, 46, 2039–2049.

Neumann, E.-R., Mysen, B.O., Virgo, D., and Seifert, F.A. (1982) Redox equilibria of iron in melts in the system CaO-Al_2O_3-SiO_2-Fe-O. Carnegie Institution of Washington Year Book 81, 353–355.

Nolet, D.A. (1980) Optical absorption and Mössbauer spectra of Fe, Ti silicate glasses. Journal of Non-Crystalline Solids, 37, 99–110.

Nolet, D.A., and Burns, R.G. (1979) Ilvaite: A study of temperature dependent electron delocalization by the Mössbauer effect. Physics and Chemistry of Minerals, 4, 221–234.

Nolet, D.A., Burns, R.G., Flamm, S.L., and Besancon, J.R. (1979) Spectra of Fe-Ti silicate glasses: Implications for remote sensing of planetary surfaces. Proceedings, 10th Lunar and Planetary Science Conference, 1775–1786.

Osborn, E.F. (1959) Role of oxygen pressure in the crystallization and differentiation of basaltic magmas. American Journal of Science, 257, 609–647.

Osborn, E.F., and Muan, A. (1960a) Phase equilibrium diagrams of oxide systems. Plate 7. The system CaO-"FeO"-SiO_2. American Ceramic Society, Columbus, Ohio.

——— (1960b) Phase equilibrium diagrams of oxide systems. Plate 10. The system CaO-"Fe_2O_3"-SiO_2. American Ceramic Society, Columbus, Ohio.

——— (1960c) Phase equilibrium diagrams of oxide systems. Plate 4. The system Na_2O-Al_2O_3-SiO_2. American Ceramic Society, Columbus, Ohio.

Presnall, D.C., and Brenner, N.L. (1974) A method for studying iron silicate liquids under reducing conditions with negligible iron loss. Geochimica et Cosmochimica Acta, 38, 1785–1788.

Riebling, E.F. (1964) Structure of magnesium aluminosilicate liquids at 1700 °C. Canadian Journal of Chemistry, 42, 2811–2821.

——— (1966) Structure of sodium aluminosilicate melts containing at least 50 mole% SiO_2 at 1500 °C. Journal of Chemical Physics, 44, 2857–2865.

Robinson, H.A. (1969) Physical properties of alkali silicate glasses: I. Additive relations in alkali binary glasses. Journal of the American Ceramic Society, 53, 392–399.

Ryerson, F.J. (1985) Oxide solution mechanisms in silicate melts: Systematic variations in the activity coefficient for SiO_2. Geochimica et Cosmochimica Acta, 49, 637–651.

Sack, R.O., Carmichael, I.S.E., Rivers, M., and Ghiorso, M.S. (1980) Ferric-ferrous equilibria in natural silicate liquids at 1 bar. Contributions to Mineralogy and Petrology, 75, 369–377.

Sato, M. (1972) Electrochemical measurements and control of oxygen fugacity and other gaseous fugacities with solid electrolyte systems. In G. C. Ulmer, Ed., Research techniques for high pressure and high temperature, p. 43–99. Springer-Verlag, New York.

Seifert, F.A., Virgo, D., and Mysen, B.O. (1979) Melt structure and redox equilibria in the system Na_2O-FeO-Fe_2O_3-Al_2O_3-SiO_2. Carnegie Institution of Washington Year Book 78, 511–519.

Seifert, F.A., Mysen, B.O., and Virgo, D. (1981) Structural similarity between glasses and melts relevant to petrological processes. Geochimica et Cosmochimica Acta, 45, 1879–1884.

——— (1982a) Three-dimensional network structure in the systems SiO_2-$NaAlO_2$, SiO_2-$CaAl_2O_4$, and SiO_2-$MgAl_2O_4$. American Mineralogist, 67, 696–718.

Seifert, F.A., Mysen, B.O., Virgo, D., and Neumann, E.-R. (1982b) Ferric-ferrous equilibria in melts in the system MgO-Al_2O_3-SiO_2-Fe-O. Carnegie Institution of Washington Year Book 81, 355–357.

Sharma, S.K., Virgo, D., and Mysen, B.O. (1978) Structure of glasses and melts of $Na_2O \cdot xSiO_2$ (x = 1,2,3) composition from Raman spectroscopy. Carnegie Institution of Washington Year Book 77, 649–652.

Spiering, B., and Seifert, F.A. (1985) Iron in silicate glasses of granitic composition: A Mössbauer spectroscopic investigation. Contributions to Mineralogy and Petrology, 90, 63–73.

Sweet, J.R., and White, W.B. (1969) Study of sodium silicate glasses and liquids by infrared spectroscopy. Physics and Chemistry of Glasses, 10, 246–251.

Takahashi, E. (1978) Partitioning of Ni^{2+}, Co^{2+}, Fe^{2+}, Mn^{2+}, and Mg^{2+} between olivine and silicate melts: Compositional dependence of partition coefficients. Geochimica et Cosmochimica Acta, 42, 1829–1845.

Thornber, C.R., Roeder, P.L., and Foster, J.R. (1980) The effect of composition on the ferric-ferrous ratio in basaltic liquids at atmospheric pressure. Geochimica et Cosmochimica Acta, 44, 525–533.

Virgo, D., and Mysen, B.O. (1985) The structural state of iron in oxidized vs. reduced glasses at 1 atm: A ^{57}Fe Mössbauer study. Physics and Chemistry of Minerals, 12, 65–76.

Virgo, D., Mysen, B.O., and Kushiro, I. (1980) Anionic constitution of silicate melts quenched at 1 atm from Raman spectroscopy: Implications for the structure of igneous melts. Science, 208, 1371–1373.

Virgo, D., Mysen, B.O., and Seifert, F.A. (1981) Relationship between the oxidation state of iron and structure of silicate melts. Carnegie Institution of Washington Year Book 80, 308–311.

Virgo, D., Mysen, B.O., and Danckwerth, P.D. (1983a) The coordination of Fe^{3+} in oxidized vs. reduced sodium aluminosilicate glasses: A ^{57}Fe Mössbauer study. Carnegie Institution of Washington Year Book 82, 309–313.

——— (1983b) Redox equilibria and the anionic structure of $Na_2O \cdot xSiO_2$-Fe-O melts: Effects of oxygen fugacity. Carnegie Institution of Washington Year Book 82, 305–308.

Watson, E.B. (1977) Partitioning of manganese between forsterite and silicate liquid. Geochimica et Cosmochimica Acta, 41, 1363–1374.

Waychunas, G.A., and Rossman, G.R. (1983) Spectroscopic standard for tetrahedrally coordinated ferric iron: γ $LiAlO_2$: Fe^{3+}. Physics and Chemistry of Minerals, 9, 212–215.

Weber, H.P., and Hafner, S.S. (1971) Vacancy distribution in nonstoichiometric magnetites. Zeitschrift für Kristallographie, 133, 327–340.

Manuscript received October 2, 1987
Manuscript accepted July 27, 1988